Martin Braarup Hansen

ENHANCING POLYMER EXCHANGE MEMBRANE WATER ELECTROLYSER'S PERFORMANCE AND EFFICIENCY BY UTILISING ELECTROMAGNETIC SOLAR RADIATION AND MAGNETIC FIELD APPLICATIONS

Hydrogen production

Thesis
CENTRIA UNIVERSITY OF APPLIED SCIENCES
Environmental Chemistry and Technology
November 2023

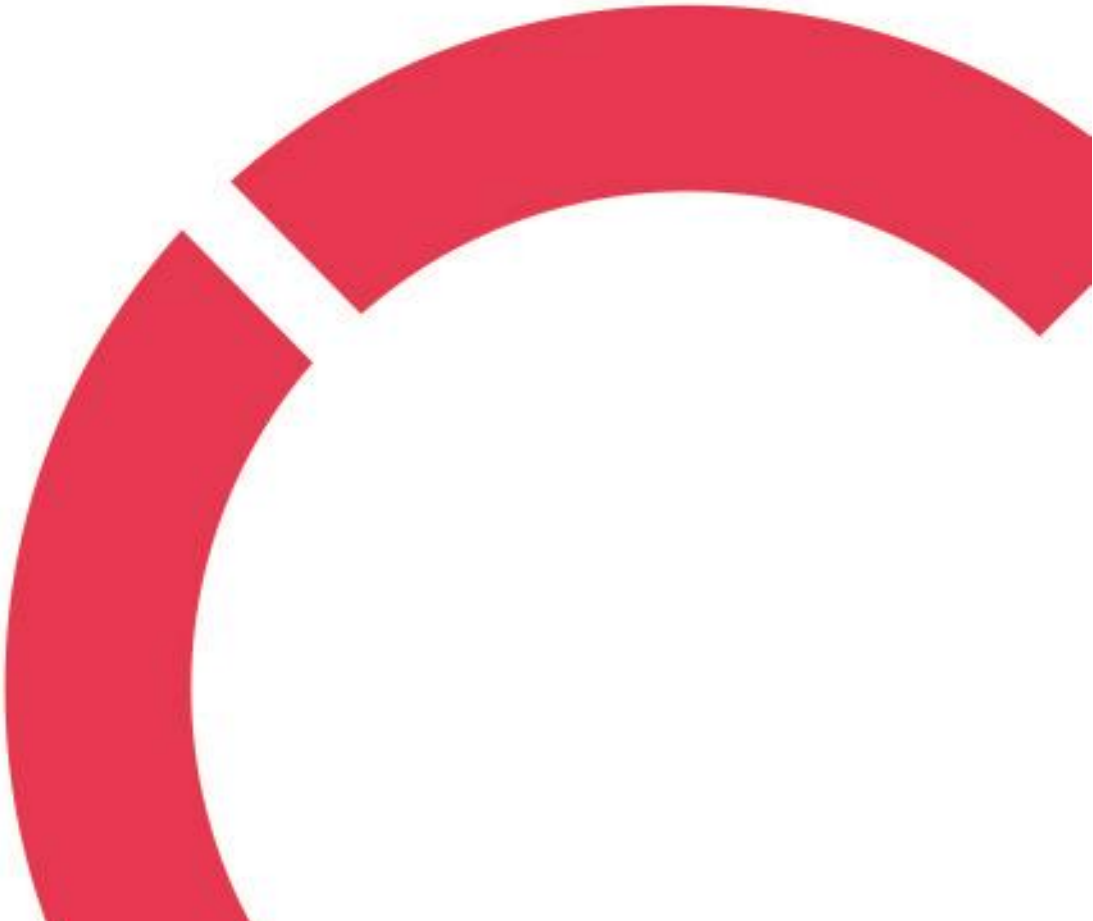

ABSTRACT

Centria University of Applied Sciences	Date	Author
	November 2023	Martin Braarup Hansen
Degree programme Environmental Chemistry and Technology		
Name of thesis ENHANCING POLYMER EXCHANGE MEMBRANE WATER ELECTROLYSER'S PERFORMANCE AND EFFICIENCY BY UTILISING ELECTROMAGNETIC SOLAR RADIATION AND MAGNETIC FIELD APPLICATIONS. Hydrogen production		
Centria supervisor Einar Nystedt		**Pages** 45 + 2

The demand for producing high-purity hydrogen gas at low cost and environmental-friendly is an ongoing topic. The polymer exchange membrane water electrolysis is a technology which can supply that demand. The technology of polymer exchange membrane water electrolysis is advancing through fields of physics exploiting electromagnetic solar radiation and magnetic fields, among others. Experimental laboratory research has significantly shown performance and efficiency improvements by applying electromagnetic solar radiation and magnetic fields separately. Electromagnetic solar radiation can excite the electrons in the water molecules to higher energy levels. Magnetic fields can remove oxygen bubbles from the electrode, reduce concentration polarisation, and enforce the proton transfer. A combination of electromagnetic solar radiation and magnetic fields has yet to be tested and documented. This work investigates experimentally the effects of electromagnetic radiation and magnetic fields separately and combined for a polymer exchange membrane water electrolysis system. The experimental work is limited to Horizon Educational Groups' polymer exchange membrane reversible fuel cell. The theoretical framework is based on photolysis, photoactive cells, photon-electron interactions, magnetic fields, magnetohydrodynamics, and Lorentz force. Former research on electromagnetic radiation and magnetic fields related to polymer exchange membrane water electrolysis is discussed. The experimental results from this work showed an enhanced current density performance for the electromagnetic solar radiation configuration and electromagnetic solar radiation and magnetic fields configuration, at 31.46% and 13.81%, respectively, compared to the standard condition. The magnetic field configuration excelled at system efficiency by 71.98% compared to the standard condition's 70.22%. Electromagnetic solar radiation has been found to increase the performance of hydrogen production by adding more energy to the system, while magnetic fields are efficient in the transfer and distribution of particles. Further research in polymer exchange membrane water electrolysis design is needed to align with the theory and principles of electromagnetic solar radiation and magnetic fields.

Keywords

electromagnetic radiation, Fleming's right hand rule, Lorentz force, magnetic field, magnetic field prepolarisation, magnetohydrodynamics, Horizon Educational Group, hydrogen production, photoelectrochemical cell, photolysis, polymer exchange membrane water electrolysis.

CONCEPT DEFINITIONS

FRHR

Fleming's Right Hand Rule

H^+

Proton(s)/hydrogen atom(s).

H_2

Molecular hydrogen gas.

HER

Hydrogen evolution reaction.

HHV

The Higher Heating Value.

LHV

Lower Heating Value.

LF

Lorentz Force

MFPP

Magnetic field pre-polarisation

MHD

Magnetohydrodynamics

NTP

Normal temperature and pressure (20˚C and 1 atm).

O

Oxygen atom(s).

O_2

Molecular oxygen gas.

OER

Oxygen evolution reaction.

PEC cell

Photoelectrochemical cell.

PEM

Polymer exchange membrane, however, usually interchangeably with *Polymer electrolyte membrane*. Both terms describe certain aspects of electrolysis, where *exchange* highlights the ability to facilitate the transfer of protons, and *electrolyte* emphasises that the membrane is the medium. The first interpretation is used for this abbreviation.

PEMWE

Polymer exchange membrane water electrolysis.

REF

The *residue electric field* is the net electric field that remains after the cancellation or subtraction of the opposing electric fields.

STP

Standard temperature and pressure (0˚C and 1 atm)

ABSTRACT
CONCEPT DEFINITIONS
CONTENTS

FIGURES

TABLES

1 INTRODUCTION

Polymer exchange membrane water electrolysis (PEMWE) is a significant area of research and development, and it is recognised as a pivotal technology for sustainable green hydrogen production. The PEMWE technology advantages include compact system design, high operating current density, and high-purity hydrogen gas. PEMWE can produce green hydrogen gas by utilising electricity generated from renewable energy sources. Hydrogen gas is essential for fuel cells. (Kumar & Hankwon 2023) Hydrogen's energy yield of 122 kJ/g is 2.75 times greater than hydrocarbon fuels (Aoualia, Becherif, Tabanjat, Emzianec, Mohammedi, Krehid, & Khellaf 2014).

The global demand for hydrogen reached 95 million metric tons in 2022 (IEA 2023). However, the demand for hydrogen in industrial sectors has tripled since 1975, and its potential as a transition fuel could lead to exponential growth in demand. Hydrogen is particularly promising for decarbonising hard-to-electrify heavy transport sectors, e.g., ships, trains, trucks, and buses. (WEF 2023) The hydrogen economy is projected to accelerate, with an estimated annual usage of 500-800 million tonnes by 2050, potentially covering 15% to 20% of global energy demand. (Forbes 2023) Despite the growing interest and investments in green hydrogen, its production still contributes to a small fraction of global hydrogen production. As of 2022, renewable and low-carbon hydrogen accounted for less than 1% of the hydrogen production globally, with a vast majority of hydrogen still being produced from fossil fuels, particularly natural gas, which accounts for approximately 75 % of the annual global hydrogen production. (IEA 2023)

Green hydrogen gas possesses significant potential as a sustainable energy vector and carrier due to its non-polluting and high calorific value. Its combustion or use in fuel cells results in zero carbon emissions. However, hydrogen production requires energy input, ideally from environmentally friendly sources. PEMWE is an alternative to the conventional approach, which uses electricity to decompose water molecules into hydrogen and oxygen. If surplus renewable energy sources power the PEMWE, the output is green hydrogen, clean energy without direct CO_2 emissions. Connecting PEMWE with e.g., solar and wind energy sources is a promising solution for utilising surplus renewable energy for green hydrogen production. It mitigates negative impacts, such as increased fossil fuel usage. (Herdem, Mazzeo, Matera, Baglivo, Khan, Congedo & Giorgi 2023)

The PEMWE technology has faced substantial obstacles, such as costs, stability issues with the electrolyser unit components, and potential damage from the anode in contact with an acidic membrane.

These issues are particularly problematic for electron conduction within the electrolyser cell, which is essential for the process. (Bystron, Vesely, Paidar, Papakonstantinou, Sundmacher, Bensmann, Hanke-Rauschenbach & Bouzek 2018) However, recent indications for PEMWE have shown significant advances in costs, efficiency, capacity, and durability in a short time. That now can compete with the most common type of electrolyser, alkaline water electrolysis. (Maier, Smith, Dodwell, Hinds, Shearing & Brett 2022)

Several studies have explored enhancing water electrolysis efficiency through various applications to alter and improve the performance and efficiency of electrolyser cells. A study by Zhao, Wang, He, Xia, Cao, Li & Sun (2023) demonstrated a 9.2% increase in hydrogen production (l/h) efficiency by using a 0.75 T magnetic field pre-polarisation (MFPP) application for alkaline electrolysis – operating within a voltage range of 42-46 V. Similarly, a study conducted by Kaya, Demir, Rees & El-Kharrouf (2020) reported a 33% current density ($A \cdot cm^{-2}$) improvement in a PEM electrolyser cell performance using a 0.5 T magnetic field application – alongside a flow rate of 300 ml min^{-1} at 2.5 V. Additionally, Bidin, Azni, Bakar, Johari, Munap, Salebi, Razak, Sahidan & Sulaiman (2016) found that directing collimated electromagnetic solar radiation at the water electrolyser cell increased the hydrogen production by 53% compared to the conventional light and dark-field setup between 0-30 V. The mentioned studies suggest that ongoing advancements in the performance and efficiency of water electrolysis are possible. The potential of combining collimated electromagnetic solar radiation and magnetism fields in enhancing PEMWE gives rise to more research.

This thesis focuses on enhancing a PEMWE cell by utilising both electromagnetic solar radiation and magnetic field applications by investigating literature and experimental research. The methodology includes collimated lenses to ensure electromagnetic solar radiation is directed at the cell and neodymium magnets to establish an external magnetic field for the PEMWE cell. The metric for measuring performance and efficiency is system efficiency, stack potential, current density and against the benchmark by Gavlik (2014). This thesis addresses the following research questions: How does electromagnetic solar radiation influence the performance and efficiency of PEMWE? How do magnetic fields impact the performance and efficiency of PEMWE? What are the combined effects of magnetic fields and electromagnetic solar radiation enhancement on PEMWE? This thesis contributes to research on the performance and efficiency of PEMWE.

The scope of this research is limited to experiments using the Solar Hydrogen Science Kit (reversible PEMWE cell) by the Horizon Educational Group (2023a), alongside additional supporting equipment

for the setup. Initially, the basic principles of PEM water electrolysis will be outlined to understand the process and system in focus. Hereafter, a theoretical overview of photolysis, photoactive cells, photon-electron interactions, magnetism, magnetic fields, magnetohydrodynamics, and Lorentz force. Next, is electromagnetic solar radiation and magnetic fields literature findings. Henceforth, is the method, results, and discussion of the conducted experiments. A reflection of the process and findings is before the conclusion.

2 POLYMER EXCHANGE MEMBRANE WATER ELECTROLYSIS

PEMWE produces hydrogen and oxygen at a ratio 2:1 (equation 1). The PEMWE efficiency against to the higher heating value (HHV) of hydrogen is 50% to 83%. The temperature for industrial PEMWE is between 50 °C and 80 °C, and the purity of hydrogen is approximately 99.9%. (Kumar & Hankwon 2022; Kumar & Hankwon 2019) On average, 50 kWh is needed to produce 1 kilogram of hydrogen (Tashie-Lewis & Nnabuife 2021), and 1 kilogram of hydrogen has a lower heating value (LHV) of 33.3 kWh (Zhang, Urantani, Hunag, Xu, Griffiths & Ding 2023).

Overall chemical reaction for a PEMWE cell:

$$2H_2O \rightarrow H_2 + \frac{1}{2}O_2 \quad (1)$$

The electrochemical water splitting can be presented by equation (2). Theoretically, a 1.23V thermodynamic cell voltage is required to drive the water splitting into hydrogen and oxygen (equation 2) at standard temperature and pressure (STP). It takes experimentally 1.48V to operate efficient water splitting at 25˚ and 1 atm to overcome ohmic resistance and kinetic energy losses. The energy losses are due to the design of the cell, components used, and electrolyte. (Kumar & Hankwon 2022)

$$H_20 + Electricity\ (237.2\ \frac{kJ}{mol}) + Heat\ (48.6\ \frac{kJ}{mol}) \rightarrow H_2 + \frac{1}{2}O_2 \quad (2)$$

2.1 Basics of Polymer Exchange Membrane Water Electrolysis

PEMWE operates by electrochemically splitting water into hydrogen and oxygen at separate electrodes (FIGURE 1.). Water is introduced at the anode, where it is split into oxygen, hydrogen ions (H+), and electrons. The hydrogen ions move through the membrane towards the cathode. Meanwhile, the electrons travel from the anode through an external power circuit, eventually recombined with the hydrogen ions at the cathode to form hydrogen gas. (Kumar & Himabindu 2019)

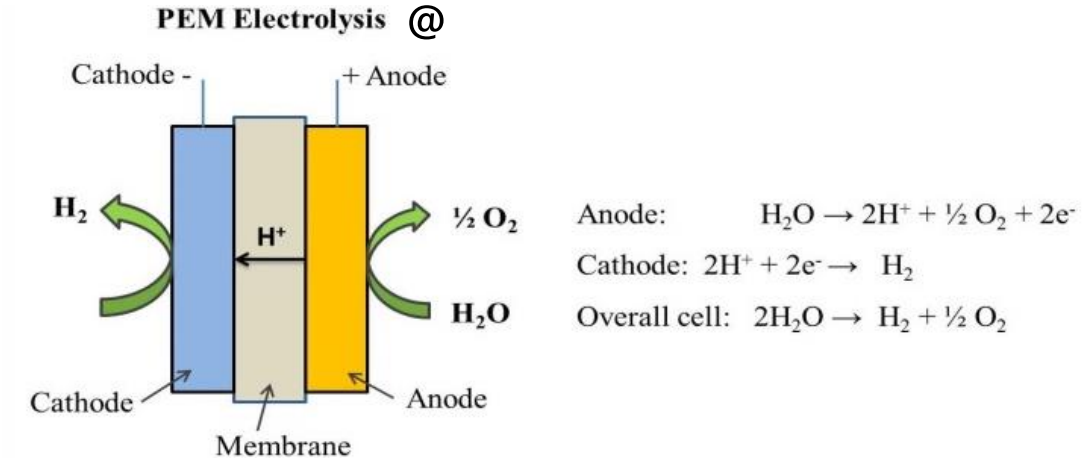

FIGURE 1. Schematic illustration of PEM water electrolysis (adapted from Kumar & Himabindu 2019).

2.2 Components and Mechanism of Polymer Exchange Membrane Water Electrolysis

The design of a PEM water electrolyser primarily includes a cell stack, which incorporates elements such as membrane electrode assemblies, current collectors, end plates, and separation plates. The core of the cell stack is composed of current collectors and bifunctional half cells; anode and cathode, which function as gas diffusion layers. Multiple PEM cell stacks are frequently integrated into a singular electrolysis system to optimise efficiency. The electrolytic membrane, primarily composed of perfluorosulfonic acid polymer, forms the structural and functional backbone of the PEM water electrolyser. It serves as a conduit for H^+ transport due to its high proton conductivity. Owing to its attributes, such as high mechanical strength, oxidative stability, and dimensional stability across diverse operational temperatures. Perfluorosulfonic acid polymer has been established as the preferred material for these membranes. Furthermore, catalysts are applied to membrane surfaces to enhance electrochemical processes. These catalysts are designed to augment the kinetics of charge transfer. This minimises the required activation energy for the electrolysis process, thereby promoting a more efficient and cost-effective system. (Kumar & Himabindu 2019)

2.3 Performance Parameters and Efficiency Measures

When evaluating the performance efficiency of PEMWE, several vital parameters are commonly examined, many of which are interrelated. The Gibbs free energy change, ΔG, involved in splitting water

into H^+ and $O^{2,}$ is an essential measure of voltage efficiency. However, the water-splitting process generates some entropy. Therefore, it is more practical to use the enthalpy change, ΔH, instead of ΔG (minimum energy needed to drive the reaction) when calculating the potential voltage requirements. Under standard conditions, ΔH equals 285.84 kJ·mol^{-1}, while ΔG is 237.22 kJ·mol^{-1}. As a result, the minimum voltage (thermoneutral voltage) required for water electrolysis can be calculated using equation (3). Voltage efficiency is the ratio of the thermoneutral voltage to the actual cell voltage. For distilled water, at a temperature of 25°C and a pressure of 1 atm, the thermoneutral voltage is 1.48V using ΔH, which gives more practical results than ΔG. For ΔG, the minimum voltage required is 1.23V at STP. Higher voltage efficiency implies less energy is wasted during electrolysis. (Kumar & Himabindu 2019)

$$V_{TN} = \frac{\Delta G}{nF} + \frac{T\Delta S}{nF} = \frac{\Delta H}{nF} \quad (3)$$

$$V_{TN} = \frac{\Delta H}{nF} = \frac{285.84 \frac{kJ}{mol}}{2 * 96500 \frac{kJ}{mol}} = 1.48V \quad (3)$$

Where,

V_{TN} = thermoneutral voltage, V

n = no. of electrons involved

F = 96500 (Faraday's constant)

ΔS = change in entropy

T = temperature

Energy is conversed, and therefore, energy conversion efficiency is essential, e.g., yields from electrical to chemical energy. Typically, the first calculation used for water electrolysis efficiency is thermoneutral voltage over cell voltage to gain an insight into what it takes to drive the electrolysis process. The formula for the electrolyser efficiency, equation (4), can be calculated using the HHV of hydrogen since water is in a liquid phase. (Kumar & Himabindu 2019)

$$\eta = \frac{V_{TN}}{V_{cell}} \quad (4)$$

Where,

V_{TN} = Thermoneutral voltage, V

V_{cell} = Cell voltage, V

The data from Horizon Educational Group for the PEM water electrolyser cell used in the Solar Hydrogen Science Kit has an efficiency of 68.1% (equation 4), based on voltage using HHV and is commonly referred to as the stack potential (Gavlik 2014). The result is in the scope of a traditional PEM single-cell electrolyser. However, multiple parameters can influence the result and what variables are included or neglected in the efficiency and performance calculations. These parameters span from the water's temperature and quality to the electrolyser's design. (Kumar & Hankwon 2022)

$$Stack\ potential\ = \frac{1.48\ V}{2.173\ V}\ =\ 0.681 \sim 68.1\% \qquad (4)$$

Since energy is conserved, the efficiency is determined by the conversion degree of electrical energy transformed into chemical energy. Operating at lower current densities typically results in higher efficiency because it lowers the operating voltages. Nonetheless, high current densities indicate a high rate of hydrogen production. However, high current densities can also lead to increased heat generation and decreased efficiency. On the other hand, faradaic efficiency in water electrolysis measures the effectiveness of electron transfer in electrochemical reactions, such as oxygen evolution reaction (OER) or hydrogen evolution reaction (HER) at an electrode's surface. Faradaic efficiency calculates the proportion of electrons contributing to the desired reaction. The ratio is determined by comparing the amount of hydrogen or oxygen gas produced to the theoretical volume, calculated using Faraday's second law, considering factors like current density, electrolysis time, and electrode area. The latter assumes a 100% Faradaic efficiency. The actual gas production can be quantified through water-gas displacement. Therefore, faradaic efficiency refers to the ratio of hydrogen produced to the theoretical amount that should be produced based on the electricity used. It reflects how effectively the electricity is being used. (Kumar & Hankwon 2022)

An electrocatalyst slurry that is created using an appropriate blend of electrocatalyst and ionomer solution, plays a dual role in enhancing water electrolysis. On the one hand, the ionomer solution promotes efficient proton transport from the electrode layers to the membrane, enhancing cell efficiency and reducing ohmic losses. On the other hand, it provides structural stability to the catalyst and improves the mechanical durability of the electrodes. The efficiency of PEMWE can be calculated on various levels. Stack efficiency represents the collective efficiency of all cells in the stack, considering factors like cell design, cooling system, and pressure losses. System efficiency can take a holistic approach, measuring the energy content of the produced hydrogen against the electrical energy input, accounting for all energy losses in the system. Lifetime or durability, often assessed in operational hours, indicates the

system's maintenance frequency or replacement need. The hydrogen production rate quantifies the volume of hydrogen produced over time, typically measured in cubic meters per hour (m^3/h). Startup time, meanwhile, denotes the duration required for the electrolyser to commence hydrogen production at total capacity from a standstill. These parameters, while individual, are also interrelated. For instance, a high current density might enhance the hydrogen production rate but negatively affect faradaic efficiency and system longevity. Consequently, optimising an electrolyser's performance necessitates a balanced approach to ensure efficient, cost-effective hydrogen production. Moreover, the components and membrane catalyst coating used for the PEM water electrolyser will affect the system and production efficiency. (Kumar & Himabindu 2019)

Electrolyser efficiency is often based on thermoneutral voltage over the cell voltage to give a simple overall representation. However, other methods to investigate a given hydrogen production's efficiency are possible based on e.g., the materials chemical properties. Many factors influence the performance of an electrolyser. A common assumption is that more expensive materials or additional equipment are needed to improve the electrolyser efficiency. It is expected to anticipate ancillary losses. Nevertheless, ohmic losses are also a topic of its own. Moreover, an approach to investigate the electrolyser efficiency involves incorporating more parameters and their involvement. Applying multiple factors in conjunction with time tends to be more challenging. An approach to understanding the efficiency includes the hydrogen-generated volume. In theory, the impact of any losses can be incorporated into a formula. Still, the effect of the system can also be calculated from comparing the results to a experimental standard by the manufacturer. Equation (5) considers the hydrogen collected volume, neglecting electricity losses. (Gavlik 2014)

$$System\ Efficiency\ = \frac{HHV \times Amount\ of\ hydrogen\ produced}{Electric\ Engergy\ Consumed} \tag{5}$$

Based on Horizon Educational Group's experimental result for the electrolyser from the Solar Hydrogen Science Kit (Gavlik 2014), the system efficiency is 55.96% (equation 5).

$$System\ Efficiency = \frac{\left(11875750\ \frac{J}{m^3}\right) \times \left(10 \times 10^{-6}\ m^3\right)}{212.22\ J} = 0.5596 \sim 55.96\% \tag{5}$$

Values used for the system efficiency calculation (5),
Time = 180 seconds
Voltage = 2.173 V

Current = 0.543 A

Power = 2.173 V × 0.543 A = 1.179 W

Electric Energy Consumed in joules = 180 seconds × 1.179 W = 212.22 J

Volume cubic meters (Amount of hydrogen produced) = 10 ml = 10 cm^3 = 10 × 10^{-6} m^3

HHV for hydrogen at NTP, density, in J·m^{-3} =141.8 $\frac{MJ}{kg} \times 10^6 \frac{J}{kg} \times$ 0.08375 $\frac{kg}{m^3}$ = 11875750 $\frac{J}{m^3}$

Calculating the system efficiency by equation (5) looks at the overall system and the result of the process rather than including phases, the design of electrolysis, or ancillary losses. Investigating ways to improve a system requires more factors and data to run detailed calculations. However, gaining data without including a more comprehensive error margin can be challenging. Nevertheless, it is possible to adjust a water electrolysis system from general theory and assumptions for how electricity works and change the metal of electrodes, e.g., to decent electricity conductors and decrease the ohmic resistance. Therefore, heavy investment can be made for a system to increase efficiency. However, it might not be economically feasible. (Gavlik 2014)

Current density is a performance indicator showing the electric current distribution across the electrode surface within a PEM water electrolyser cell. It is defined as the amount of electric current flowing per unit area of the electrode surface that can be expressed in amperes per square centimetre (A·cm^{-2}) as shown in equation (6). This metric is instrumental in determining the efficiency and performance of the electrolysis process, making it a vital parameter for optimisation. (Kumar & Hankwon 2022)

$$Current\ density = \frac{I}{Area} \quad (6)$$

Values used for the current density calculation (6),

I = Current, A

Area = Cell, cm^2

Based on Horizon Educational Group's experimental result for the electrolyser from the Solar Hydrogen Science Kit (Gavlik 2014), the current density efficiency is 0.087 A·cm^{-2} (equation 6).

$$Current\ density = \frac{0.543\ A}{5.76\ cm^2} = 0.087\ \frac{A}{cm^2} \quad (6)$$

Hydrogen has the highest gravimetric energy density compared to all other known substances, with an LHV of 120 $MJ \cdot kg^{-1}$ (Møller. Jensen, Akiba & Li 2016). LHV is a helpful metric for evaluating the potential for water splitting. Assuming no losses, a voltage of 1.23 V is required for the reaction, based on Gibbs' free energy calculation. (Kumar & Himabindu 2019) When assessing the electrolysis cell's system efficiency using liquid water, the HHV is a more accurate metric than the LHV. This is because the HHV accounts for the enthalpy change, which is linked to the phase transition of water from liquid to vapour, an energy cost that the electrolysis system must withhold. Therefore, HHV offers a more comprehensive view of the system's thermodynamic performance. (Buitendach, Gouws, Martinson, Minnaar & Bessarabov 2016)

2.4 Challenges and Limitations of Polymer Exchange Membrane Water Electrolysis

Contamination in water can harm the PEMWE. The contamination can lead to membrane degradation and mechanical damage. The membrane develops pinholes due to chemical degradation over time. The chemical degradation of the membrane leads to a decline in efficiency and eventual system failure. Therefore, using appropriate water quality is crucial for maintaining the performance, efficiency, and longevity of PEMWE. (Xing, Li & Avgouropoulos 2021)

Despite the benefits of PEMWE, the technology encounters the high cost of its components. Central to the electrolyser’s efficiency and durability are the membranes. By reducing the thickness of the membranes while bolstering their mechanical strength, both efficiency and durability can be enhanced, leading to lower electricity consumption. The electrocatalyst materials, which rely on expensive elements like platinum and iridium oxide, must be resolved. Substituting or minimising these precious materials with earth-abundant alternatives and optimising surface properties for better reaction kinetics is an alternative. Stackability is a significant cost factor, mainly due to using platinum or gold-coated titanium in components like porous transport layers and bipolar plates. High internal resistance would also impact the system’s performance and must be kept at a minimum. Moreover, the process can generate heat, and effective thermal management is necessary to prevent overheating, which can damage the membrane and other components. (Kumar & Hankwon 2022)

3 ELECTROMAGNETIC SOLAR RADIATION

Sunlight, electromagnetic solar radiation, is a natural energy source which consists of photons. Photon are a quanta of light exhibiting particle or wave properties according to the experimental circumstances. Photons carry energy based on their frequency and wavelength. Among two photons, the one with the higher frequency or shorter wavelength will have higher energy. The electromagnetic spectrum is divided into ranges of wavelengths, from shorter, e.g., ultraviolet, to longer wavelengths, e.g., infrared (FIGURE 2.). Electromagnetic solar radiation comprises a wide range of photons with different wavelengths and frequencies. The specific distribution of wavelengths in electromagnetic solar radiation gives rise to its characteristic colour and properties. (Urone, Hinrichs, Dirks & Sharma 2012) Around 4-5% of the electromagnetic solar radiation entering the Earth's atmosphere has a wavelength corresponding to the ultraviolet region of the electromagnetic spectrum (from 300 nm). About 45% is in the visible range (400–760 nm), and the rest ~50% is at and near the infrared regions. (Malato-Rodríguez 2004)

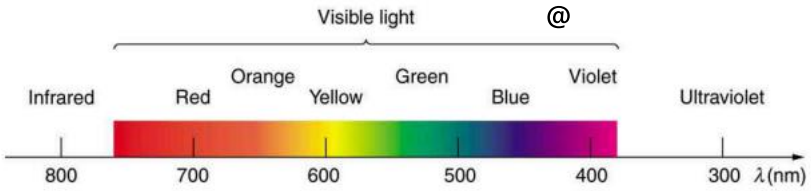

FIGURE 2. Part of the electromagnetic spectrum (adapted from Urone et al. 2012)

Regarding frequency, electromagnetic solar radiation shows a corresponding range of frequencies inversely proportional to the wavelength. Higher-frequency electromagnetic solar radiation corresponds to shorter wavelengths. In contrast, lower-frequency electromagnetic solar radiation corresponds to longer wavelengths. The frequency of electromagnetic solar radiation is between 10^{14} and 1.10^{15} Hz. The amount of energy which a photon holds is directly proportional to its frequency. The equation E = h*f, where E (joules) represents energy, h is Planck's constant (6.626×10^{-34} joule-seconds), and f is the frequency (hertz) is used to calculate the amount of energy which a photon holds. Ultraviolet rays carry more energy per photon than lower-frequency waves like infrared rays. Electromagnetic solar radiation with a higher frequency contains more energy per photon than electromagnetic solar radiation with a lower frequency. (Urone et al. 2012) In water molecules, photons can be absorbed to break the bonds between hydrogen and oxygen. This process is called photolysis, also known as photodissociation or photodecomposition. (Speight 2018)

3.1 Principles of Photolysis

Photolysis, which is a part of photochemistry, refers to the process of breaking down chemical bonds via photon interaction. A photolysis reaction results from transferring energy using photons directly or indirectly, breaking down the chemical bonds. The effect of photolysis is subjected to chemical adsorption properties, reactivity, and strength of electromagnetic solar radiation. The process of photolysis is separated into three phases. First, using water molecules as an example, electromagnetic solar radiation adsorption excites the electrons in the water molecules to move to a higher energy state or leave the atoms, which changes the molecule's electronic configuration. It is, secondly, undergoing a photochemical transformation or deexciting the electron. The adsorbed energy can lead the electrons to break or form chemical bonds. Fundamentally, the molecules seek to return to a more stable energy state. Thirdly, the thermal reactions of intermediate molecules generated during the second phase can undergo further reactions. This third phase is driven by heat rather than the electromagnetic solar radiation energy itself. The reactions taking place reflect the conditions under which photolysis is performed. Before the photolysis process can initiate, the molecule that has adsorbed the electromagnetic solar radiation energy must return to a lower energy state. This happens typically via fluorescence, where the molecule releases energy. Any leftover energy is quickly lost through collisions with other molecules. However, it can also happen that the energy is transferred to another molecule instead of being lost through quenching to a molecule with a lower energy state. Some chemicals accept easier transferred energy than others, and this can lead to the overall photolysis process slowing down. Sensitised photolysis uses certain chemicals as catalysts that capture electromagnetic solar radiation energy and transfer it to target molecules. This can subsequently enhance the photolysis rates. Any photon with sufficient energy can initiate the photolysis chemical reaction and is not limited to visible light. (Speight 2017)

Collimated electromagnetic solar radiation ensures that the photons move in parallel directions, effectively focused on a specific point or path (FIGURE 3.). This alignment allows for the concentration of their energy, facilitating efficient photon-electron interactions and maximising the effect. Collimation does not change the electromagnetic solar radiation's intensity, frequency, or wavelength. Instead, collimation enhances the directionality and alignment of the electromagnetic solar radiation waves. This allows the photons to be effectively focused on a targeted area. Convex lenses can collimate electromagnetic solar radiation with different focal lengths. (Bidin et al. 2016)

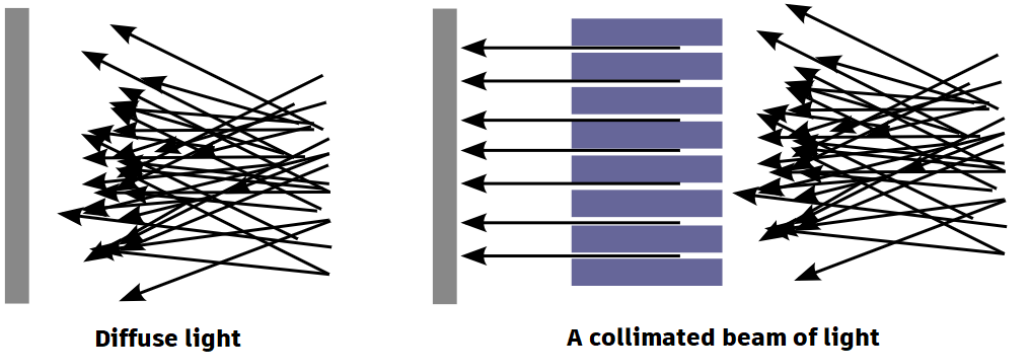

FIGURE 3. Diffuse and collimated light

3.2 Mechanisms of Photon-Electron Interaction

The energy state of the atom before and after interactions with electromagnetic solar radiation stays the same. The electron moves to a higher energy level when absorbing the photon, and when emitting the photon, the electron will return to a lower energy level. However, elastic scattering can occur in which a photon is absorbed and then instantaneously reemitted by the electron. The energy, both incoming and outgoing, of the photon is conserved in elastic scattering but is typically emitted in a new direction. The electron of the atom gains the momentum needed to ensure the conservation of momentum. The change of direction of the photon without changing the energy level of the electron is the essential characteristic of elastic scattering. Both directly and indirectly, elastic scattering is nature's most common photon-electron interaction, which counts almost for all the scattering of electromagnetic solar radiation in natural waters. Nevertheless, inelastic scattering can also occur naturally, like in deep ocean waters, which generate a significant amount of yellow and red radiation. Elastic and inelastic scattering is fundamental in how electromagnetic solar radiation interacts with matter (FIGURE 4.). While elastic scattering conserves its electromagnetic solar radiation energy after the electron interaction, inelastic scattering loses. Since the photon via inelastic scattering loses electromagnetic solar radiation energy, resulting in a higher wavelength or lower frequency, this would change the colour of the scattered photon's electromagnetic solar radiation. It is also possible for photons to pass matter without an interaction. As a note, anti-inelastic is another phenomenon where the photon is emitted with higher energy due to a lower wavelength or higher frequency. Anti-elastic scattering is less common. However, it is possible under certain conditions, such as high temperature, in which electrons are at a higher energy state. The photon-electron interaction is essential in many physical systems, from basic atomic and molecular processes to advanced technologies like lasers. (Jonasz & Fournier 2007)

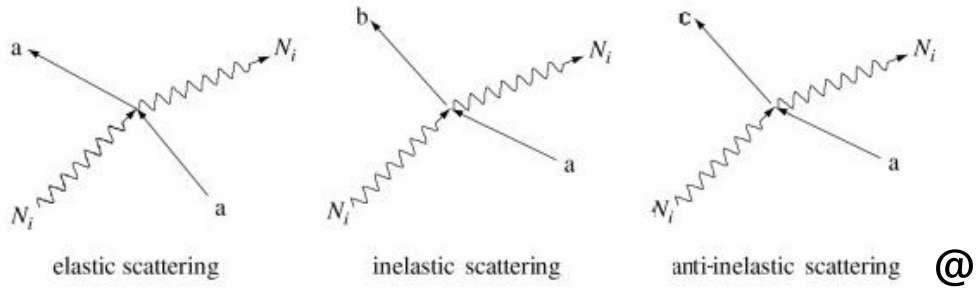

FIGURE 4. Light scattering (adapted from Jonasz et al. 2007)

3.3 Photoactive Cells

Photoactive cells utilise photons for splitting water molecules into the components of hydrogen and oxygen. This is achieved by generating excited electrons and pairs of electron holes. However, there are different setups of photoactive cells, each employing a distinct method to facilitate this water-splitting process. One type of cell, the photocatalytic cell (FIGURE 5.), can produce hydrogen by exploiting the photocatalytic properties of specific materials, such as titanium dioxide. In this process, the photocatalyst absorbs the photons from electromagnetic solar radiation, creating excited electrons and electron-hole pairs. These particles subsequently participate in redox reactions; electron holes oxidise water to produce oxygen gas, and excited electrons reduce protons to produce hydrogen gas. Despite this, photocatalytic processes often underperform when compared to direct electrolysis methods, mainly due to the challenges in preventing the recombination of the electron-hole pairs. To address this underperformance, a photocatalytic cell can be combined with an electrolyser to form a photoelectrochemical (PEC) cell. This setup increases the separation of the electron-hole pairs by applying a bias voltage and electric field, enhancing the water-splitting process's effectiveness. This additional voltage, the photovoltaic effect, assists in overcoming the energy barriers associated with water-splitting. The photovoltaic effect reduces the recombination of electron-hole pairs, potentially leading to a more efficient hydrogen production process. A PEC cell typically includes photoactive electrodes. The material of the electrodes generates electron-hole pairs when it absorbs electromagnetic solar radiation, and the resulting electrons reduce water to form hydrogen. However, this process's efficiency largely depends on effectively separating and collecting the generated charges, which poses significant challenges. Moreover, finding a suitable semiconductor material that can use a substantial portion of the electromagnetic solar radiation spectrum is another challenge. For a photocatalytic system to capture electromagnetic solar radiation effectively, it needs a minimum of 1.23 electron volts (eV) corresponding to approximately 1000 nm of the electromagnetic solar radiation spectrum. In theory, various types of water could be used for photoactive cells, e.g., salt water. (Idriss 2020)

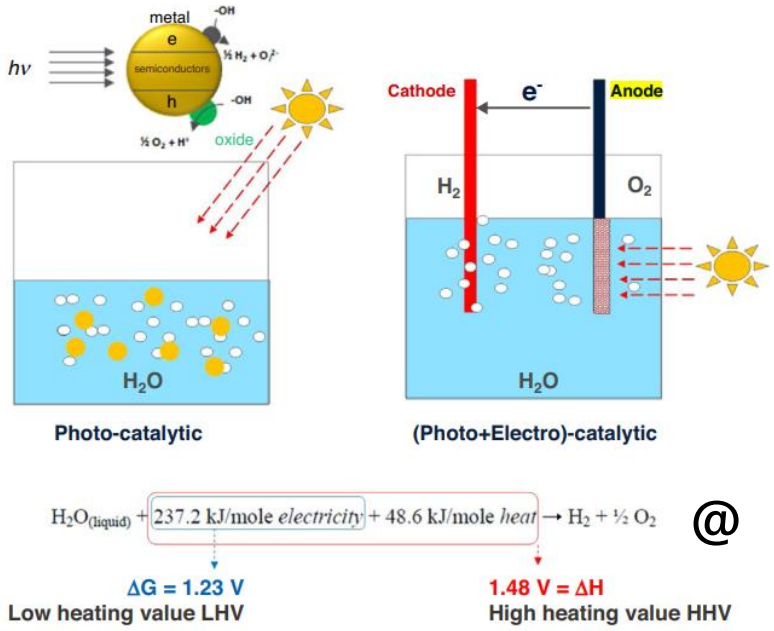

FIGURE 5. Schematic description of photocatalysis & photoelectrocatalysis (adapted from Idriss 2020)

3.4 The Photon-Electron Interaction Effect on Activation Energy for Photoactive Cells

The concept of activation energy is a fundamental aspect of chemical kinetics. Activation energy is a thermodynamic parameter that quantifies the energy barrier that reactant molecules must overcome to proceed from the initial state to the transition state during a chemical reaction. The theory of activation energy is based on the collision theory and transition state theory. According to collision theory, reactant molecules must collide with sufficient energy and proper orientation for a chemical reaction to occur. The minimum energy needed for a successful collision is the activation energy. Molecules with energies below activation energy cannot overcome the energy barrier and will not proceed to the product state. Transition state theory provides a more detailed and quantitative description of the reaction process. This intermediate state forms during the reaction when the reactant molecules are in a high-energy configuration and have partially broken and formed chemical bonds. The transition state represents the highest energy point, and its energy equals the activation energy. In the context of photon-electron interaction on activation energy, the adsorption of photons by reactant molecules can lead to electronic excitation and higher energy levels for the electrons. This elevated energy state allows the reactant molecules to access higher-energy configurations, which may facilitate the formation of the transition state and overcome the activation energy barrier. By lowering the activation energy, photon-

electron interaction can enhance the reaction rates and promote the occurrence of photochemical reactions even under moderate conditions. Understanding activation energy and its relation to photon-electron interaction is vital for designing and optimising electromagnetic solar radiation-driven chemical processes. The activation energy theory, rooted in collision theory and transition state theory, provides a theoretical framework to understand the role of energy barriers in chemical reactions. The effect of photon-electron interaction on activation energy is a critical factor in photochemical processes, enabling more efficient energy conversion. (Flowers, Theopold, Langley & Robinson 2019)

4 MAGNETIC FIELDS

Magnetism corresponds to a unique physical property governed by magnetic fields. Five main types of magnetism are ferromagnetic, ferrimagnetic, antiferromagnetic, paramagnetic, and diamagnetic. Ferromagnetic materials represent the most observed. Ferromagnetic objects have a strong attraction to magnetic fields. Elements with ferromagnetic properties are iron, nickel, cobalt, gadolinium, and neodymium, together with their alloys. Furthermore, ferromagnetic materials can be transformed into magnets, creating magnetic fields. (Kong, Liu, Yang, Li, Zhang & Wang 2018) Magnets have two poles: a north and a south magnetic pole. Unlike poles attract and like poles repel. This similarity also applies to electrostatic charges. (Urone et al. 2012) Several factors dictate permanent magnets' strength, including material composition, saturation magnetisation, size, shape, magnetisation process, grain structure, coercivity, temperature, and external magnetic fields. Moreover, the strength of the permanent magnets also depends on the overall application and context. (MacCallum, Lewis, Skomski, Kramer & Anderson 2014)

A magnetic field is characterised by invisible forces exerted by an object, enabling it to influence another object from a distance without a visible physical link. The field represents the force-producing object – magnetic fields illustrate magnetic forces. Fundamental principles for magnetic fields have been established through magnetic field lines (FIGURE 6.). However, these lines are not physical entities. The direction of the magnetic field aligns tangentially with its field line at any specific point. The magnetic field's strength also relates to its field lines' concentration. It relates directly to the count of lines in a unit area perpendicular to those lines. Also, magnetic field lines never cross, guaranteeing a distinct field value at each point in space. Also, these field lines are continuous, forming unbroken loops running seamlessly from the north pole to the south pole. (Urone et al. 2012)

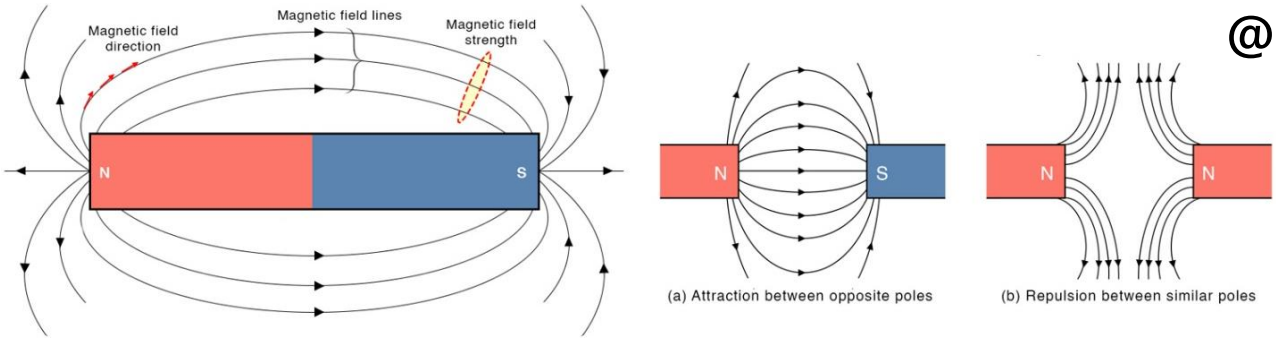

FIGURE 6. Magnetic field lines generated by a magnetic bar (adapted from Urone et al. 2012)

4.1 Magnetohydrodynamics

Magnetohydrodynamics (MHD) and its effect is a physical phenomenon that combines magnetofuild dynamics/hydromagnetics and electromagnetism. The core concept of MHD is that magnetic fields can generate current in a flowing conductive fluid, e.g., water, which then produces forces on the fluid and alters the original magnetic field. Therefore, MHD combines magnetism and fluid dynamics principles to describe how magnetic fields and fluid flows interact and influence each other. In simple terms, MHD is an application where magnetic force pumps fluids despite not having any moving mechanical parts. (Sheikholeslami & Ganji 2016)

Fleming's Right Hand Rule is used to visualise (FIGURE 7.) and determine the direction of an induced current/electromotive force, motion/force, and magnetic field (Harun, Tuli & Mantri 2020). FRHR is in effect when the conductor, e.g., fluid, moves perpendicular to a magnetic field. FRHR is connected to MHD through the principles of electromagnetism regarding the interaction of magnetic fields and moving fluids. At the same time, MHD provides a complex framework for understanding the behaviour of conducting elements in magnetic fields. Then FRHR offers a quick and intuitive way to determine the direction of interactions between induced current/electromotive force, motion/force, and magnetic field. Therefore, FRHR can be helpful when describing the MHD theory and setting up experiments. (Urone et al., 2012)

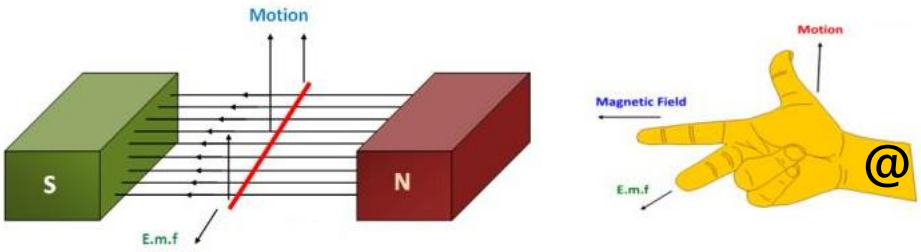

FIGURE 7. Fleming's Right Hand Rule (adapted from Urone et al., 2012)

4.2 Lorentz Force

MHD studies the behaviour of conducting fluids when influenced by magnetic fields. At the centre of MHD is the Lorentz Force (LF) a force exerted on moving charged particles due to simultaneous electric and magnetic fields. In the context of MHD, the LF becomes pivotal. As conducting fluids move

relative to a magnetic field, they generate an electromotive force, leading to an induced electric current. When these electric currents encounter magnetic fields, whether the original or external ones, they are subjected to the LF defined as the cross-product of the electric and magnetic fields (Carlton 2019). This interaction between electric and magnetic fields impacts the fluid's flow dynamics. The equation E = qE+qv*B, where F is the force, E is the electric field, v is the velocity, B is the magnetic force, and q is the charged particle, gives the force exerted on the charged particle. (Hughes 2004) The LF influences how a conductive fluid responds to the combined effects of pressure, viscosity, and electromagnetic forces, revealing the complex dynamics observed when conducting fluids meet magnetic fields. (Whites 2005)

MHD propulsion is a technique that employs electric and magnetic fields to generate thrust. In MHD propulsion, the conductive fluid is accelerated using electromagnetic forces to create thrust. The LF is the primary mechanism behind electromagnetic propulsion. When charged ions and electrons in a fluid are subjected to this force, they move. Utilising this movement can be used for propulsion e.g., a fixed coil generates a magnetic field in a ship powered by electromagnetic propulsion. This magnetic field interacts with an electric current, originating from electrodes at the ship's base and passing through the surrounding water. The resulting interaction creates a force based on the Lorentz law, propelling the ship forward. More precisely, the force exerted on charged particles arises from their reaction to the electric field and their movement within the magnetic field. When these electric and magnetic fields align perpendicularly, the resulting force propels the ship in the intended direction. MHD propulsion capitalises on the synergy between electric currents and magnetic fields to produce movement/thrust. (Carlton 2019)

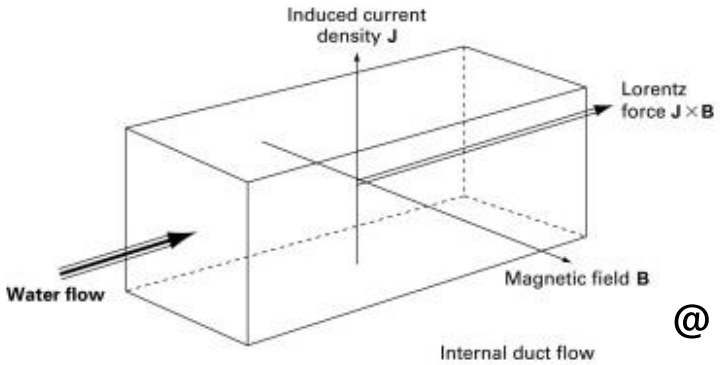

FIGURE 8. Principle of magnetohydrodynamics propulsion (adapted from Carlton, 2019).

4.3 Electric and Magnetic Fields Effect on Water Electrolysers

Oxygen gas bubbles are produced at the electrodes and membrane during water electrolysis. Incorporating magnetic fields can speed up the separation of these gas bubbles from the anode and membrane surfaces. This acceleration occurs through LF and MHD, reducing ohmic pressure drop and increasing reaction overpotential. (Zhao et al. 2023) The presence of magnetic fields also alters the behaviour of the oxygen gas bubbles, which LF influences to detach and rise more quickly. A change in the flow pattern can affect the performance and efficiency of the electrolysis process in either a positive or negative direction. However, magnetic fields can enhance mass transfer rates at the electrodes, leading to improved performance and efficiency. Moreover, an altered flow can contribute to a more uniform temperature distribution within the electrolyser and avoid higher temperatures. Given the complexity of MHD effects in water electrolysis, careful experimental methods are essential for accurately capturing this phenomenon. (Kaya et al. 2020)

In systems where electricity is applied under the influence of magnetic fields, the phenomenon known as Residue Electric Field (REF) may occur. REF is the net electric field that remains after the cancellation or neutralisation of opposing electric fields. When electrical power is applied to the electrolyte, local charges, including ions and water dipoles, align against the external electric field, reducing its overall strength. This counter-alignment makes water electrolysis for hydrogen production less efficient. (Bidin et al. 2016)

A typical water electrolyser is not designed to function as an electromagnetic propulsion system. However, the ions produced during the electrolysis process do move under the influence of an applied electric field. If this ion movement is controlled using an external magnetic field, a force could be generated through the action of LF. For this approach to be feasible, several considerations must be addressed, such as system scalability, efficiency, fluid flow stability, and safety. (Gotzig, Wurdak & Harmansa 2022)

5 PREVIOUS RESEARCH

Studies by Zhao et al. (2023) and Kaya et al. (2020) indicate that magnetic fields increase water electrolysis performance and efficiency under certain experimental circumstances. The authors behind the two studies highlight rising CO_2 emissions to call for action, which green hydrogen could act upon, especially water electrolysis. They point out the high purity level of hydrogen produced as an advantage, which has increased the interest in further development of the technologies. However, both point to the operating costs as a downside, which needs decreasing to make technologies more competitive. Moreover, both conclude upon their experimental research that using magnetic fields can increase the performance and efficiency of water electrolysers even on an industrial level. Kaya et al. (2020) note that other fields of physics have been introduced to researchers in pursuit of increasing the performance and efficiency of water electrolysers, and the main categories are supergravity, ultrasonic and magnetic fields. However, a third study by Biden et al. (2016) pointed out that sunlight, electromagnetic solar radiation, can also be considered to increase the performance and efficiency of water electrolysis. According to Biden et al. (2016), experiments using electromagnetic solar radiation directly at the water electrolysis process have a high potential to enhance renewable hydrogen production to fight energy crises and environmental pollution.

5.1 Magnetic Field Research

Zhao et al. (2023) research focussed on the MFPP method to achieve increased performance and efficiency of an alkaline water electrolyser system. The MFPP is designed to integrate with a high-power industrial alkaline water electrolyser system. To validate the effectiveness and applicability of the MFPP method, the researchers used simulations to finalise the parameters and then constructed the application. The MFPP application was included in a comprehensive industrial system-level verification version. The team had a 22-cell electrolyser setup, an MFPP application, a circulation pump, gas-liquid separation units, purification systems, cooling and heat exchange, and an automatic control cabinet. The system's performance was tested based on current and voltage characteristics, and efficiency was evaluated on hydrogen production yield. Their results from these tests confirmed that the MFPP method was effective. The performance of MFPP was further assessed by comparing its efficiency across a range of voltage levels, specifically from 40 V to 46 V. During these tests, both pressure and flow rate were kept consistent 1.3 MPa and 200 L/h respectively. The magnetic field strength was maintained at about 0.75 T, and the electrolyte temperature was between 70 ˚C and 90 ˚C. The findings

revealed that, at its peak, the MFPP method could enhance hydrogen production efficiency by 9.2 %. The measured current and voltage characteristics were found to be in alignment with the hydrogen production rates as measured by a flowmeter. The theories which support the MFPP method are LF and MHD. Magnetic fields can potentially affect the behaviour of the gas bubbles during electrolysis. By applying LF and MHD, these fields accelerate the detachment of bubbles from electrodes and membrane surfaces. This acceleration leads to a decrease in both ohmic pressure drop and reaction overpotential. When a magnetic field is present, there is not only a reduction in the average size of the bubbles but also a tighter distribution of bubble sizes. Furthermore, introducing a magnetic field during the electrolysis process augments the rising speed of the gas bubbles. Apart from these effects on gas bubbles, magnetic fields also impact the inherent properties of liquid water. They can alter the water's physical and chemical characteristics, including viscosity, enthalpy, and surface tension. When it comes to solutions, the electrical conductivity of a NaCl solution, for instance, increases in the presence of a magnetic field. (Zhao et al. 2023)

Kaya et al. (2020) research highlights the impact of using magnetic fields to enhance the performance of PEMWE. By integrating a magnetiser with a transparent PEMWE cell, the study systematically observed how magnetic fields, ranging from 0 T to 0.5 T, influence the PEMWE's efficiency across water flow rates from 100 ml/min to 300 ml/min. The core mechanism behind this improvement is the LF induced by the magnetic field. This force facilitates the efficient removal of oxygen bubbles from the electrolyser, reduces concentration polarisation, and consequently increases the overall performance. Notably, at a magnetic flux density of 0.5 T and a 300 ml/min flow rate at 2.5 V, the electrolyser's efficiency current density increased by 33% compared to its regular operation without a magnetic field. However, the MDH effect occurred due to LF, and the buoyancy force contributed positively since both LF and MDH were applied. Beyond the performance, removing oxygen bubbles through the magnetic field can extend the electrolyser's lifespan. This is due to the minimised interaction between the oxygen produced and the materials of the anode. Furthermore, the diameter of the gas bubbles was observed to become smaller and more accessible to remove from the anode. The operational setup was meant for laboratory use. The design incorporated a transparent PEMWE cell to maximise magnetic permeability. Moreover, an electromagnet was used to control magnetic flux densities, ensuring accurate and interference-free measurements. The consistency behind the enhanced PEMWE results across various magnetic flux densities and water flow rates indicates a potential for integrating magnetic fields in PEMWE operations, especially at low rates where the impact of the magnetic field becomes more definite. (Kaya et al. 2020)

5.2 Electromagnetic Solar Radiation Research

Biden et al. (2016) research focused on solving the REF, which leads to inefficient electrolysis systems. The researchers thought of utilising electromagnetic solar radiation to overcome the problem. Their experiment was conducted with a transparent electrolysis chamber containing 100 ml of distilled water catalysed with 1.0476 mg of NaCl. Additionally, 7 ml of ethanol was added, and a molybdenum plate served as a reagent. This setup was exposed to three distinct lighting conditions: a dark field created by wrapping the chamber in black paper, direct conventional electromagnetic solar radiation, and collimated electromagnetic solar radiation achieved with a high-reflective mirror combined with two convex lenses, with respective focal lengths of 80 mm and 10 mm. The collimated electromagnetic solar radiation beam was directed at the anode in the electrolysis chamber with a beam diameter of approximately 8 mm. Due to the challenging nature of controlling natural electromagnetic solar radiation, an alternative source was used: a halogen lamp with a wavelength range of 360-1500 nm, 5 W/0.2 A. Using a halogen lamp, signals were captured at 480 nm (blue), 580 nm (yellow), and 650 nm (red), with green light (495-570 nm) not absorbed in the water due to its high intensity among the white lights. Based on this experimental observation, a green laser source was used to stimulate the collimated electromagnetic solar radiation in the primary research of enhancing the performance and efficiency of an electrolyser system. One key measurement was the surface tension, which determined the electric field's impact on water molecules. It was hypothesised that a stronger electric field would amplify the surface tension. The researchers recorded the hydrogen production for 10 minutes, resulting in 16 ml with the dark-field, 31 ml under conventional electromagnetic solar radiation, and 53 ml with collimated electromagnetic solar radiation. From their analysis based on the obtained results, it was clear that water's molecular structure, which features an electric dipole due to the hydrogen and oxygen atoms' asymmetric alignment, is fundamental. Breaking the hydrogen bond is essential for electrolysis, while conventional electromagnetic solar radiation influences hydrogen production primarily through temperature elevation. Collimated electromagnetic solar radiation directly reinforces the electric field, optimising the water-splitting process. The research team concluded that collimated electromagnetic solar radiation significantly enhances hydrogen production from water electrolysis. Their findings suggest that the inherent polarizability of sunlight can be utilised to strengthen the electric field during electrolysis, catalysing water splitting. The data from surface tension and electrical conductivity measurements further emphasise this effect of electromagnetic solar radiation's potential.

6 ELECTROMAGNETIC SOLAR RADIATION AND MAGNETIC FIELD EXPERIMENTS

As part of the thesis work, experiments were conducted to analyse the effect of electromagnetic solar radiation and magnetic fields on a PEMWE cell. Five configurations for the experiments were used, partially inspired by the work of Kaya et al. (2020) and Biden et al. (2016): no-alterations, dark-field, solar, magnets, and solar & magnets. For each configuration, five tests were conducted. The experiments are performed with a small-scale PEM water electrolyser and related equipment, which do not correspond to the effect that commercial standards would obtain. The experiments took place on October 20th and 21st of October in Kokkola, Finland. According to the Finnish Meteorological Institute's radiation observations point in Ruukki (approximately 150 km northeast of Kokkola), the diffuse radiation the 21st of October between 14:00 and 16:00 was 2.3-2.4 $W \cdot m^{-2}$ during the time of experiments involving electromagnetic solar radiation (Finnish Meteorological Institute 2023). The general room temperature was 18˚ Celsius. Regarding safety measurements safety glasses, gloves, a coat, and a fire blanket were available during the experiments. Precautions handling electric equipment and hydrogen gas were taken. However, due to limited electrical input and output (maximum of 3 V) and the small amount of gas (10 ml), no further extensive hazardous assessment or report was completed due to very low-risk levels. No safety data sheet was completed since the only substance used was distilled water, and hydrogen gas, which is flammable, is taken into consideration. Good laboratory practice was upheld.

6.1 Experimental Setup

The equipment and materials used for the experiments have many components. The Solar Hydrogen Science Kit (reversible single PEMWE cell) by the Horizon Educational Group includes a PEMWE cell, two gas containers, a 3 V power supply, tubes, a syringe, plugs, and small platforms. Two neodymium magnets with a hole (5.5 mm diameter), zinc galvanised, 10 x 6 x 1.2 cm (approx. 1 T) were used. Both a double-Convex Lens, 35 x 82 mm Focal length, Grade 1. and a double-Convex Lens, 17 x 9 mm Focal length, Grade 1. were used. Also, a metal rack for magnets to hang from was used. A mirror to reflect the sunlight was applied. One telescope #1 to mount the lenses for adjusting the light plot, and another telescope #2 to mount the mirror. Two digital multi-meters for measuring the voltage and current were used. A laboratory elevation rack was used to lift the platform of the electrolyser system. A platform for the electrolyser system was also used. A stopwatch to take time and a video recorder to

capture the time and measurements. Four plastic strips for magnets to be mounted to the metal rack. Distilled water was utilised. Two soldering iron stands were used to fix the positions of the multi-meters' banana plugs. A black towel was used for the dark-field tests. An infrared laser to measure the surface temperature of the anode side of the PEMWE cell was utilised. FIGURE 9. is a general overview of the setup used for the laboratory experiments. Variations to the setup were made depending on the configuration used.

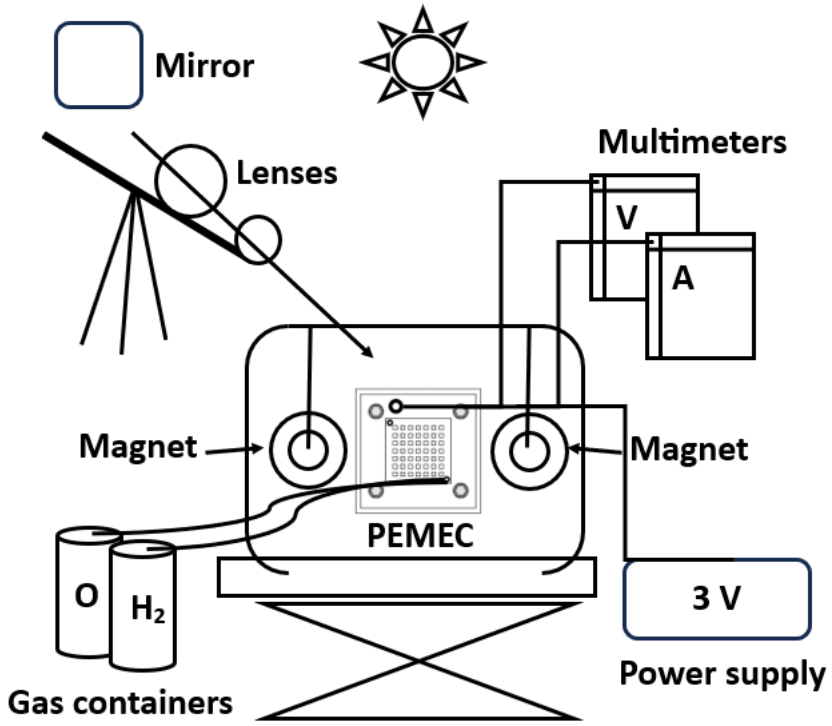

FIGURE 9. Representation of the laboratory setup

6.2 Experimental Procedure

Depending on the configuration, the tests were managed in different ways. However, the initial steps of preparing were the same. First, the PEMWE cell was filled with distilled water by a syringe at the anode side via a smaller tube. The distilled water had time to settle, and more was added until a steady cover of the anode appeared, approximately 1 ml, and the tube was closed. Another small tube was added to the cathode side to release gas, if necessary. Two other tubes were connected to the PEMWE cell and hydrogen and oxygen gas containers. The power supply was connected via the negative banana plug to the cathode side of the PEMWE cell, and its positive banana plug was fixed in series with the multimeter measuring the current. The multimeter measuring current was directly inserted into the anode side of the PEMWE cell. Besides, a second multimeter measuring voltage was fixed parallelly at

each side of the PEMWE cell. The setup would be controlled from the power supply by an on/off button, activating the water-splitting process, and the multimeters would also start working. The values from the multimeters would be recorded on video together with the time. When 10 ml of hydrogen gas was collected, the test would end, resulting from water displacement, by visual observation. After a successful operation, the gas containers would be emptied, and the PEMWE cell would be refilled. Batteries (2*1.5 V) would be changed after each configuration. For the configuration No-alterations, the system was operated by the initial steps. A black towel was used for the Dark-field configuration on top of the initial steps. The solar configuration used additional equipment such as a telescope with lenses mounted upon it and a telescope with a mirror mounted to it. Sunlight was reflected via the mirror to the lenses to create a light beam (approximately 10 mm in diameter) directed at the anode side covering the electrode area. For the configuration of the magnets, they were placed so the north pole towards the cathode and the south pole towards the anode side of the PEMWE cell. The magnets were placed according to FRHR. The magnets had a span of approximately 5 cm. The solar and magnets configuration was a combination of these two individual configurations.

6.3 Data Collection, Measurements and Calculations

The data obtained from tests based on the five configurations are available in APPENDIX 1. The collected data includes voltage and current in relation to time. The data were video recorded and inserted into Microsoft Excel in intervals of 15 seconds plus the finishing time and value when 10 ml of hydrogen gas were collected. Additionally, the temperature of the surface of the anode side of the PEMWE cell was measured as random samples. The temperature measurements occurred from the beginning to the end of each configuration, and a temperature range was established. Resistance (equation 7) and power (equation 8) can be calculated by having values for voltage and current. Both resistance and power are used for the system's performance based on the relationship between the voltage and current. Having values for time and power makes it possible to calculate the electric energy consumption by equation (9).

$$Resistance, R\ (Ohms) = \frac{Voltage,\ V\ (V)}{Current,\ I\ (A)} \tag{7}$$

$$Power, W\ (Watts) = Voltage,\ V\ (V) * Current,\ I\ (A) \tag{8}$$

$$Electric\ energy\ consumption\ (J) = time * power\ (W) \quad (9)$$

The stack potential equation (4), system efficiency equation (5), and the current density equation (6) are ideal to perform based on the data obtained from the configuration tests. Moreover, the of use Gavlik's (2014) results, which are from Horizon Educational Group's teaching materials, as a benchmark for equations (10) and (11). Five tests were conducted for each configuration, and the average was taken for the calculations and results. The data, calculations and results are presented in tables except for the current density, which will be displayed in two graphs compared to voltage (FIGURE 10) and time (FIGURE 11). The data and calculations for current density are available in APPENDIX 2. The temperature is shown as the range, which is not used directly in the calculations.

$$Performance\ vs. Benchmark = (180\ s/time) * (212.22\ J/electric\ energy\ consumption) \quad (10)$$

$$System\ efficiency\ vs. Benchmark = system\ efficiency * (180\ s/time) \quad (11)$$

7 RESULTS

The results presented below are computed in Microsoft Excel based on the configuration test data available in APPENDIX 1. A ranking will also appear in multiple tables to be used in the discussion part. TABLE 1. shows the average measurement of the data collected based on each configuration. TABLE 2. presents the calculated resistance and power by equations (7) and (8), respectively, for each configuration. TABLE 3. is the calculation of each configuration's system efficiency by equation (5). TABLE 4. shows a performance efficiency indicator of each configuration versus Gavlik's (2014) results as a benchmark using equation (10). TABLE 5. displays the system efficiency for the configurations of each configuration versus Gavlik's (2014) results as a benchmark using equation (11). TABLE 6. is the calculated stack potential for each configuration. TABLE 7. are the configurations against standard configuration.

TABLE 1. Collected configuration data @ 10 ml H_2

Configurations	Cell temperature range (˚C)	Time (sec.)	Voltage (V)	Current, I (A)
No-alterations	15.5-16.7	125.8	1.842	0.730
Dark-field	15.1-16.3	134.6	1.801	0.698
Solar	18.5-19.9	100.0	1.865	0.956
Solar & Magnets	18.5-19.7	113.6	1.870	0.833
Magnets	15.5-16.11	128.2	1.819	0.711

TABLE 2. Configurations resistance and power @ 10 ml H_2

Configurations	Resistance (Ohms) = V/I	Power (W) = V*I	Ranking by minimum resistance	Ranking by maximum power consumption
No-alterations	2.524	1.344	3	3
Dark-field	2.586	1.260	5	5
Solar	1.952	1.782	1	1
Solar & Magnets	2.245	1.559	2	2
Magnets	2.572	1.287	4	4

TABLE 3. System efficiency for the configurations @10 ml H_2

Configurations	Time (sec.)	Hydrogen gas collected (ml)	Power (Watts) = V*I	Electric energy consumption (J) = time*W	System efficiency (%) = (HHV*Amount of hydrogen)/Electric energy consumed*100	Ranking by highest efficiency
No-alterations	125.8	10	1.344	169.12	70.22	2
Dark-field	134.6	10	1.260	169.62	70.01	3
Solar	100	10	1.782	178.23	66.63	5
Solar & Magnets	113.6	10	1.559	177.06	67.07	4
Magnets	128.2	10	1.287	164.98	71.98	1

TABLE 4. Performance efficiency for the configurations @ 10 ml H_2 - benchmark (Gavlik 2014)

Configurations	Time (sec.)	Electric energy consumption (J) = time*W	Performance vs. Benchmark = (180/time)*(212.22/electric energy consumption)	Ranking by highest performance
No-alterations	125.8	169.12	1.7955	4
Dark-field	134.6	169.62	1.6731	5
Solar	100	178.23	2.1433	1
Solar & Magnets	113.6	177.06	1.8992	2
Magnets	128.2	164.98	1.8061	3

TABLE 5. System efficiency for the configurations @ 10 ml H_2 - benchmark (Gavlik 2014)

Configurations	Time (sec.)	System efficiency (%) = (HHV*Amount of hydrogen)/Electric energy consumed*100	System efficiency vs. Benchmark (%) = system efficiency*(180/configuration time)	Ranking by highest efficiency
No-alterations	125.8	70.22	100.48	4
Dark-field	134.6	70.01	93.63	5
Solar	100	66.63	119.94	1
Solar & Magnets	113.6	67.07	106.28	2
Magnets	128.2	71.98	101.07	3

TABLE 6. Stack potential @ 10 ml H_2 - thermoneutral 1.48 V

Configurations	Voltage (V)	Stack potential (%) = (Thermoneutral V / cell V) *100	Ranking by the highest potential
No-alterations	1.842	80.35	3
Dark-field	1.805	81.98	1
Solar	1.865	79.35	4
Solar & Magnets	1.870	79.13	5
Magnets	1.819	81.34	2

TABLE 7. Configurations against the standard condition % @ 10 ml H_2

Configurations	Time (sec.)	Voltage (V)	Current, I (A)	$A \cdot cm^{-2}$
No-alterations	-	-	-	-
Dark-field	-7.00	-1.99	-4.36	-6.28
Solar	20.51	1.26	30.93	31.46
Solar & Magnets	9.70	1.54	14.18	13.81
Magnets	-1.91	-1.22	-3.09	-6.25

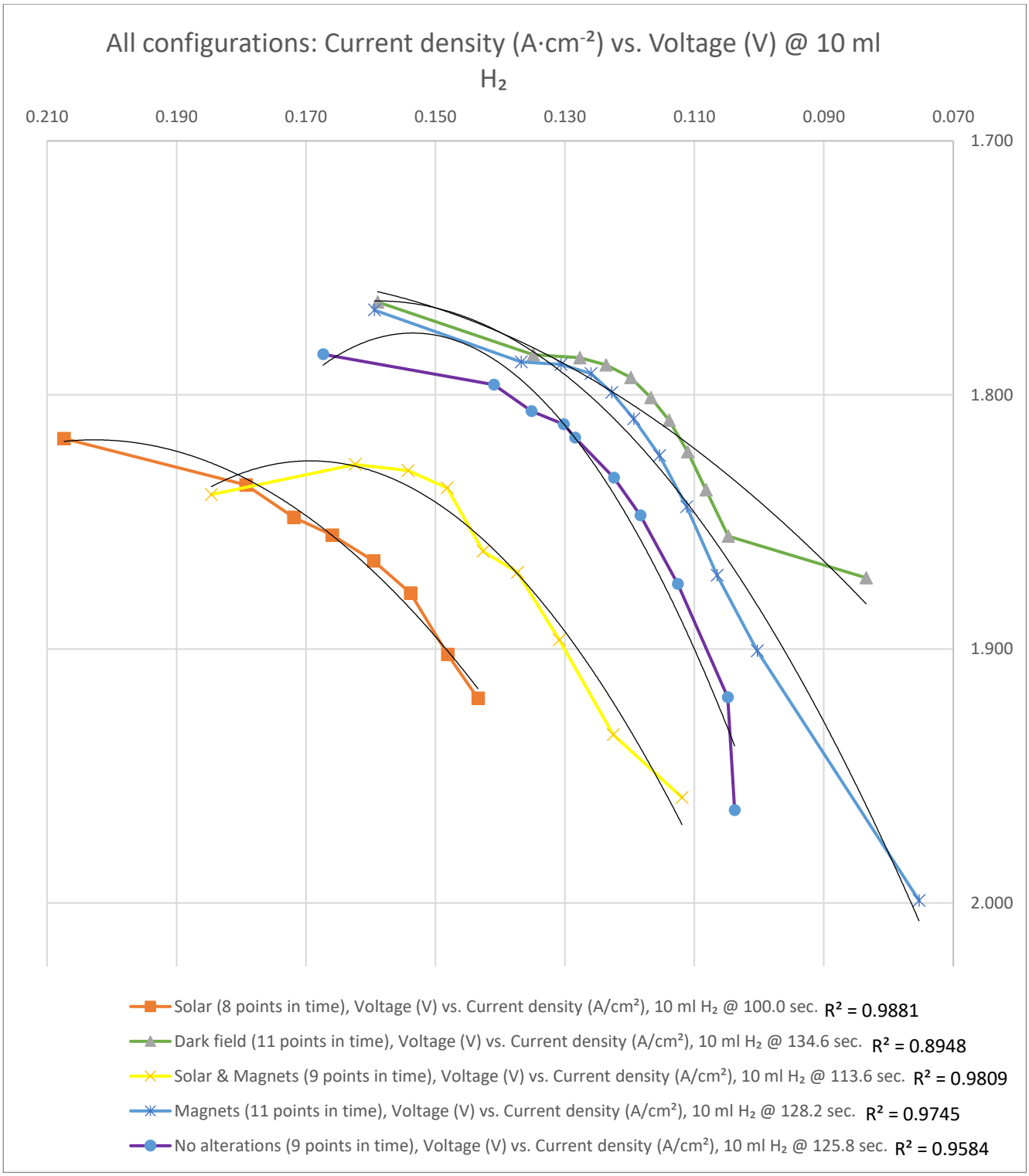

FIGURE 10. Graph of all configurations: Current density (A·cm^{-2}) vs. Voltage (V) @ 10 ml H_2

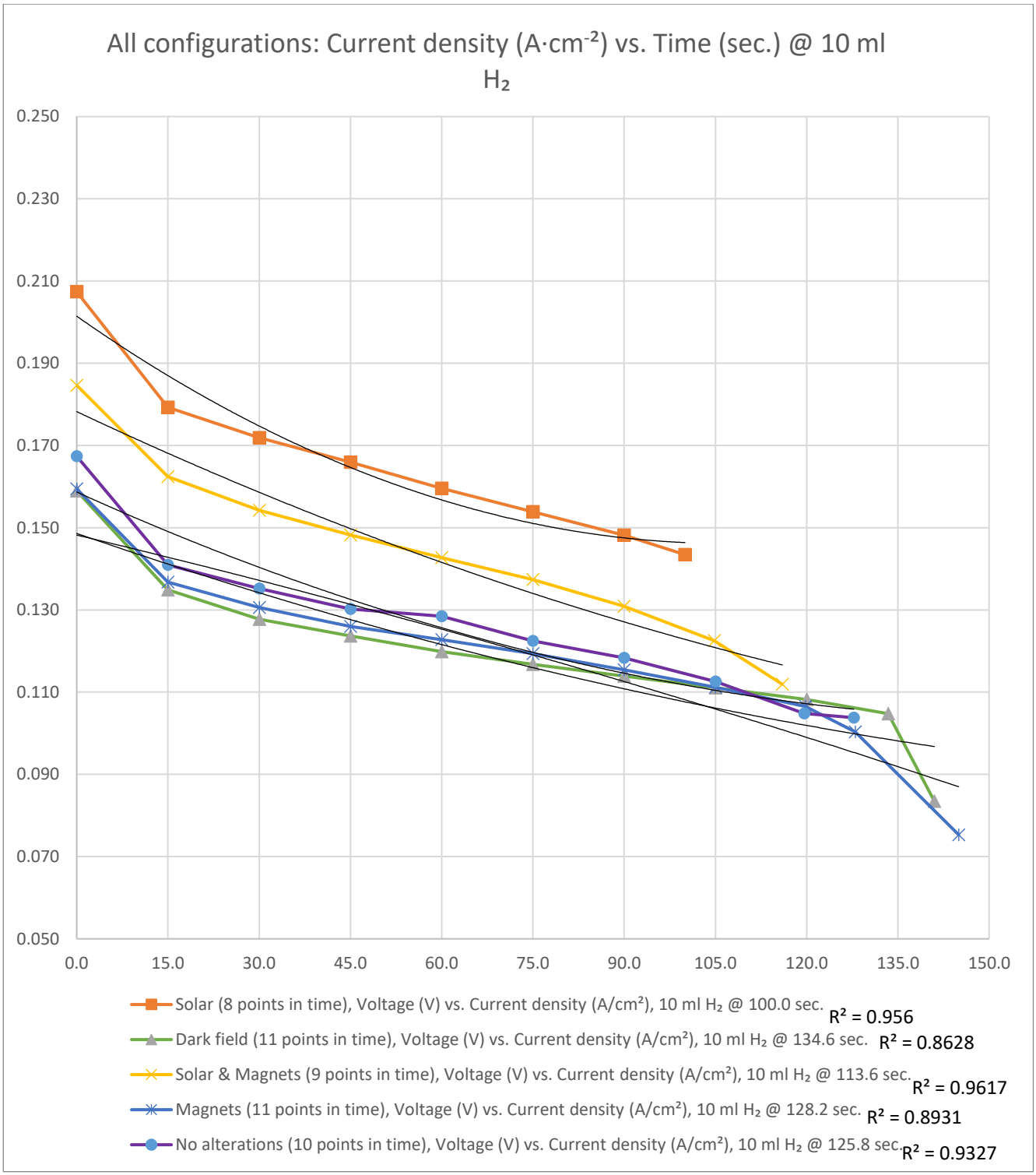

FIGURE 11. Graph of all configurations: Current density (A·cm^{-2}) vs. Time (sec.) @ 10 ml H_2

8 DISCUSSION

TABLE 1. shows the solar and solar and magnets configuration's temperature range above the rest, between 18.5-19.9 ˚C and 18.5-19.7 ˚C, respectively. This higher temperature range indicates the influence of electromagnetic solar radiation exposure on the PEMWE cell's temperature. In contrast, without electromagnetic solar radiation involvement, the dark-field configuration tends to maintain lower temperatures in the range of 15.1-16.3 ˚C. Biden et al. (2016) state that collimated electromagnetic solar radiation amplifies the overall effective electric field. A stronger integrated electric field is beneficial as it enhances hydrogen production efficiency from water electrolysis. Yet, the stronger the electric field imposed by electromagnetic solar radiation, the better the alignment achieved, causing the water molecules to experience stress and stretching. Moreover, these molecular changes can be observed by measuring the water's surface tension. Furthermore, Biden et al. (2016) also point out that when water is heated, its molecular behaviour undergoes changes that enhance hydrogen production. As the temperature rises, the movement of water molecules intensifies due to an increase in their average kinetic energy. This energy increase weakens the hydrogen bonds. Additionally, the dielectric properties of water, which relate to its ability to transmit an electric field, are altered with this reduced bond strength. As a result, water molecules gain more freedom to oscillate, bend, and eventually break free from their hydrogen bonds.

The time to reach 10 ml H_2 varies among configurations (TABLE 1.). The solar configuration was faster by an average of 100.0 seconds. On the opposite end, the dark-field configuration took 134.6 seconds on average. All configurations experienced a drop in hydrogen production towards the 10 ml point. The main reason is the concentration overpotential. As the electrolysis process continues, the water concentration decreases near the electrode surface, leading to a potential drop that can reduce the PEMWE cell's efficiency. This is related to the current density of the system (Kumar & Hankwon 2022).

Voltage measurements (TABLE 1.) further underline the electromagnetic solar radiation impact with 1.865 V and 1.870 V for solar and solar and magnets, respectively. The electromagnetic solar radiation exposure is linked to an upsurge in voltage. The lowest voltage is observed for the dark-field configuration, measured at 1.805 V. The solar configuration results in a peak current of 0.956 A, emphasising the prominent role of electromagnetic solar radiation exposure in amplifying the electric current. When solar and magnets are combined, there is a slight drop in current and an extension in time compared to

the Solar configuration. Interestingly, magnets are not far from the standard condition, no-alterations, when not combined with solar. The more significant positive impact of LF and the buoyancy effect for separating the bubbles of the anode seems to have difficulties compared to Kaya et al. (2020) observations using FRHR. The introduced magnetic field by the magnets should reduce the mass transfer losses at the electrodes and should result in MHD created by LF. The limited LF could be due to the lack of free flow of the electrolyte and pressure – or the cell's overall design. No pump, additional distilled water or moving water flow was used during the experiments. However, when an electric current moves through a magnetic field, it is subjected to LF. Furthermore, based on their research, Kaya et al. (2020) state that if the water flow rate increases, the gas bubbles have less time to interact with the magnetic field, so a sufficient magnetic flux is needed to observe the LF effect. Zhao et al. (2023) point out that a study highlighted that the bubble coverage fraction is notably diminished in the presence of an external magnetic field. Moreover, the influence of an alternating magnetic field on its conductivity is even more effective compared to a steady magnetic field. Kaya et al. (2020) also state the evolution of oxygen gas bubbles can create a barrier, preventing new electrolytes from reaching the electrode surface. This barrier can cause additional voltage requirements and reduce efficiency. This can result from LF and the buoyancy effect operating vertically in opposite directions at the anode instead of supporting each other in the same direction in removing the gas bubbles. Meanwhile, the electric current pushes the gas bubbles horizontally towards the anode. It makes it harder for the gas bubbles to escape if LF and the buoyancy effect are not in direction alignment. The magnet field used for the configurations experiments in this thesis was also stronger, 1 T, compared to Zhao et al. (2023) 0.75 T and Kaya et al. (2023) 0-5 T.

Biden et al. (2016) also state that when electricity is applied to water, the water reacts and creates its opposing electric fields. These opposing fields reduce the effectiveness of the applied electric field. This is due to the phenomenon of REF, which also reduces hydrogen production efficiency. Essentially, the water's electrical properties oppose the electricity applied, making the process less efficient. Experimental data here suggests that solar exposure plays a pivotal role in influencing the cell's parameters, with enhancements seen in temperature, voltage, and current. The integration of magnets with solar application seems to moderate this, but the role of magnets alone remains mainly comparable to the standard condition, no-alternations.

TABLE 2. shows that the solar configuration is the most efficient, having the lowest resistance at 1.952 Ohms. This translates to it also having the highest power, registering at 1.782 W. Essentially, with its low resistance, the solar configuration allows for more effortless electric current flow, leading

to a higher rate of energy usage. On the other hand, the dark-field configuration lacks performance, showing the highest resistance of 2.586 Ohms. This increased resistance correlates with its lowest power consumption of 1.260 W, marking it as the least active or reactive among the configurations tested. Interestingly, when magnets are introduced alongside electromagnetic solar radiation exposure in the solar & magnets configuration, there is an increase in resistance to 2.245 Ohms. However, it maintains a commendable power consumption of 1.559 W, positioning it second in efficiency and power usage following the solar configuration. Ranking fourth, the configuration of the magnets falls between the configurations of no-alterations and dark-field. However, the dark-field configuration appears least favourable due to its high resistance. Nevertheless, the solar and solar and magnets numbers express more power, resulting in a faster process. However, the extra energy does not come from the power supply but from the photons' contribution.

Kumar & Hankwon (2022) point out that the additional voltage required for efficient water-slitting is to overcome the kinetics and ohmic resistance in the PEMWE cell. The ohmic losses are because of the resistance of the electrolyte and any connectors or conductive materials used in the cell. As electric current flows through the electrolyser, these resistive components heat up, wasting energy as heat. Zhao et al. (2023) say the cell(s) of the electrolysers are designed to reduce resistance and energy consumption. The magnetic field treatment is not taken into design consideration, which would affect parameters such as viscosity, conductivity, surface tension, enthalpy, and hydrogen bonding.

In TABLE 3. the configuration of the magnets was the most efficient, achieving 71.98% system efficiency (equation 5) while consuming the least electric energy at 164.98 J. This means that the magnet configuration was the most proficient in producing hydrogen for every unit of electricity consumed. On the other end of the spectrum, the solar configuration, despite its high-power usage of 1.782 W, was the least efficient with a system efficiency of 66.63%, closely followed by the configuration solar and magnets of 67.07%. It also had the highest electric energy consumption of 178.23 J, indicating that more power does not equal higher efficiency. It must be noted that external energy was added to the system for the solar and solar and magnets configurations, resulting in a photoelectrochemical effect. In between, the no-alterations and dark-field configurations were closely matched in efficiency at 70.22% and 70.01%, respectively. Based on Kumar & Hankwon (2022), research shows commercial PEMWE has an efficiency between 50% and 83%, so all the configurations used are presented within that range.

TABLE 4. expresses the configurations compared to Gavlik's (2014) benchmark, with weight on time and electric energy consumption to reach the 10 ml mark of H_2 (equation 10). Among all configurations, the solar configuration demonstrated the best performance, which was 2.1433 times better than the benchmark. This suggests that under electromagnetic solar radiation conditions, the system operates most efficiently relative to the Gavlik benchmark despite having a higher electric energy consumption of 178.23 J compared to the other configurations. The solar and magnets configuration was the second best performing, with a performance score of 1.8992. Interestingly, its energy consumption was close to that of the solar configuration, showcasing the potential benefits of combining solar energy with magnetic elements. The magnets configuration came in third with a performance score of 1.8061. With the least electric energy consumption at 164.98 J, it balances efficiency and power conservation. The no-alterations configuration, the standard condition for the configurations, with a score of 1.7955, ranked second last. Lastly, the dark-field configuration, with a performance of 1.6731, was ranked fifth, making it the least efficient relative to Gavlik's benchmark.

TABLE 5. examines the configurations, focusing on system efficiency, for producing 10 ml of H_2 against Gavlik's (2014) benchmark. The system efficiency metrics were calculated using equation (11), considering the system's efficiency and the weight of the time taken for each configuration against the benchmark. The solar configuration was the top performer, even with a system efficiency rate of 66.63%. When adjusted against the benchmark, its efficiency spiked to 119.94%, making it the most efficient configuration relative to the benchmark. This achievement is notable, especially given its relatively short configuration time of 100 seconds. The solar and magnets combination followed in second place, with an efficiency of 67.07%. After benchmark adjustment, its performance stood at 106.28%. This indicates the synergy of solar energy with magnetic properties, resulting in enhanced system performance. The magnets configuration ranked third with an efficiency of 71.98%, the highest among all configurations. However, after adjusting for the benchmark, it settled at 101.07%. Its configuration time of 128.2 seconds possibly played a pivot role in its relative performance drop. The no-alterations configuration, which is the standard condition, achieved a system efficiency of 70.22% that makes it fourth in the ranking. Its benchmark-adjusted efficiency was 100.48%. Lastly, is the dark-field configuration with a system efficiency of 70.01%. Once benchmark-adjusted, its efficiency dropped to 93.63%. This drop suggests that even with acceptable system efficiency, its longer configuration time, 134.6 seconds, negatively affects its performance against Gavlik's (2014) benchmark. There is less focus on the consumed energy for the configurations using equation (11) compared to equation (5) since system efficiency does not consider the external energy added to the system, as in the case of solar and solar and magnets.

TABLE 6. shows the stack potential (equation 4), H_2 volume of 10 ml, and set against a thermoneutral voltage of 1.48 V. Stack potential is a key performance indicator, determining the ability of the water-splitting process to take place. The dark-field configuration is ranked highest, with a stack potential of 81.98%. With a voltage measurement of 1.805 V, this configuration has maximised the potential to produce hydrogen. This was followed by the configuration of magnets, with a stack potential of 81.34% and a voltage of 1.819 V. The performance of the magnet configuration shows the magnetic fields influencing hydrogen production, with a positive outcome. The no-alterations configuration, the standard condition, ranks third with a stack potential of 80.35% and a voltage of 1.842 V. This ranking highlights that a foundational setup can achieve acceptable efficiency levels without specific alterations. The solar configuration ranks fourth, with a stack potential of 79.35% and a voltage of 1.865 V. The solar & magnets combination is ranked last despite combining electromagnetic solar radiation and magnetic fields. Its stack potential stands at 79.13%, with a voltage measurement of 1.870 V. Nevertheless, the configurations are very near each other and high. However, the stack potential only does take one primary variable into account, which results in limited insight. Kumar & Himabindu (2019) point out that stack potential is rather an indicator of overcoming the overpotential needed to drive the water-splitting, which is the combined overpotential for HER and OER.

FIGURE 10. shows the voltage and current density relationship across the configurations to reach 10 ml of H_2. The solar configuration, depicted by the orange curve, has the highest R^2 value of 0.9881, indicating a near-perfect relationship between voltage and current density. This suggests that the solar configuration is highly predictable. The dark-field configuration, represented by the green curve, has an R^2 value of 0.8948. The solar and magnets combination, represented by the yellow curve, has an R^2 value of 0.9080. The magnets configuration, represented by the blue curve, has an R^2 value of 0.9745. Lastly, the no-alterations configuration, standard condition, is represented by the purple curve and has an R^2 value of 0.9584. All configurations display strong correlations between voltage and current density. The solar configuration stands out as the most efficient in terms of energy conversion. This analysis highlights the importance of understanding the impact of each configuration to optimise hydrogen production systems effectively.

FIGURE 11. shows the relationship between current density and time for the five different configurations. The solar configuration starts at 0.207 $A \cdot cm^{-2}$ and with the most significant initial drop, 29 $A \cdot cm^{-}$

², hereafter, a consistent decrease, settling at 0.143 A·cm^{-2} by 100 seconds later. This configuration exhibits a strong fit between the data and its model with an R^2 value of 0.956. The dark-field configuration starts at 0.159 A·cm^{-2} and declines towards 0.0.83 A·cm^{-2} by 135 seconds later. Its R^2 value stands at 0.8628, the lowest among the configurations, but still indicates a reasonably tight correlation. The solar and magnets configuration begins at 0.185 A·cm^{-2} and ends at 0.112 A·cm^{-2}, 113 seconds later. The R^2 value for this setup is 0.9617, the highest among the configurations. The magnet configuration began at 0.159 A·cm^{-2} and stopped at 0.075 A·cm^{-2} 145 seconds later, with an R^2 value of 0.8931. The no-alterations configuration initiates at 0.167 A·cm^{-2} and ends at 0.104 A·cm^{-2} 125 seconds later, with an R^2 value of 0.9327. The solar and magnet configuration came out with the strongest relationship between current density and time.

FIGURE 10. and 11. showcase the current density relationship with voltage and time, respectively. However, the average current density for each configuration gives further insight into the energy conversion. The solar configuration is the top performer with an average of 0.166 A·cm^{-2}, followed by solar and magnets with 0.144 A·cm^{-2}, no-alteration 0.126 A·cm^{-2}, magnets 0.119, and dark-field 0.118. solar was the most predictable in its relationship to voltage. However, solar and magnets exceeded the relationship with time. However, both are very near to each other prediction-wise, but they differ in current density. Kaya et al. (2020) observed that increasing the magnetic flux density from 0 T to 0.1 T at different water flow rates would significantly enhance the current density in the PEMWE cell. However, when increasing the magnetic flux from 0.1 T to 0.5 T, only a minor change in the performance was detected at 2.5 V. Kumar & Himabindu (2019) point out that a commercial PEM water electrolyser, which uses a Nafion membrane (the same type used for testing the five configurations), can reach a current density of 2 A·cm^{-2}. The configurations are far from reaching 2 A·cm^{-2}, which puts the experimental setup in perspective. TABLE 7. sums up the configurations against the standard condition, no-alterations, for operation time, voltage, current, and current density.

9 REFLECTION

A pattern emerged from analysing the five configuration results and the perspectives from former research and literature. Eventually, it takes multiple parameters to evaluate the performance and efficiency of the five configurations. It matters how the performance and efficiency are measured and presented. Therefore, it is advised to clearly state or reference how it is done to help the readers. An extension formula that includes the power from electromagnetic solar radiation would support a more detailed approach to system efficiency calculation. From a statistical perspective, the standard deviation calculations could contribute to a more coherent statical work. More tests of each of the five configurations would yield more evidence. However, it would benefit from measurement software to handle the volume of data.

The configuration data for solar and solar and magnets faced difficulties since the measuring equipment could not tell what energy was added to the system from electromagnetic solar radiation. However, the standard condition would somewhat support the claim for solar and magnets. Further investigations between the configurations would indicate values. However, due to a limited framework and variables, direct comparison among the configurations would not come with absolute values.

Moreover, a pyranometer in series with both solar configurations would eventually give more precise data while running the tests. A pyranometer can receive and convert the power from electromagnetic solar radiation into units per area. The measurement output from a pyranometer can be expressed in $W \cdot cm^{-2}$ (Kambezidis. 2012). Measurements like this could be included in calculating performance and efficiency.

The solar configuration setup for the PEMWE cell has similar capabilities as a photocatalytic cell. The PEMWE performed as a semiconductor for the photons and, therefore, could generate a voltage. As mentioned earlier, this is referred to as a PEC cell achieving a photoelectrochemical effect. This effect provides the energy to excite the electrons in water or at the electrodes to assist with the water-splitting process, which increases the separation of the electron-hole pairs (Idriss 2020). Biden et al. (2016) state the advantage of replacing the collimated electromagnetic solar radiation with a laser source. The green light on the electromagnetic spectrum was observed not to be absorbed in water, making it a good substitute for testing electromagnetic solar radiation in water electrolysis in a laboratory. This

revelation from Biden et al. (2016) could also be considered for further research. However, the objective here was to use the natural source of electromagnetic solar radiation. It should be mentioned a two-layer of window glass separated the electromagnetic solar radiation before being reflected by a mirror for both solar configurations. The PEMWC cells need to be constructed of a material which allows photons to travel through to the water-splitting that is taking place, e.g., transparent plastic.

The magnets used for the tested magnet configurations were stronger, 1 T, compared to Zhao et al. (2023) 0.75 T and Kaya et al. (2023) 0-5 T. This could have influenced the outcome of tests, and only one distance between was applied approximately 5 cm. As mentioned, no moving water or additional pressure by a pump occurred for the configurations. Therefore, tests with different distances and magnets with different strengths could provide further insight.

Based on the results and the raised discussions, more research into electromagnetic solar radiation and magnetic fields would benefit PEMWE. Other external forces, such as ultrasonic (Kaya et al. 2020), could also be added for testing. A holistic point-of-view approach advocates conducting further research and treating the findings accordingly. The next step can be to verify the findings from the tested configurations by further testing with Horizon Education Group or other peers.

Ongoing research could include the paramagnetism for O_2 as a subtopic in relationship to PEMWE. Paramagnetism is a magnetic behaviour in which the substance is weakly attracted to an externally applied magnetic field. The underlying reason why oxygen is paramagnetic is due to its unpaired electrons, and since the electrons are spinning, it gives them a magnetic movement. Therefore, when the O_2 is exposed to a magnetic field, its unpaired electrons will align with the field, resulting in a weak attraction to it (Fardell et al. 2010). Kaya et al. (2020) notes the paramagnetic property of O_2, which changes the gas bubbles' direction in the magnetic field.

The setup used for the five configurations costs approximately 250 EUR, which is assumed to be lower compared to the setup used for Biden et al. (2016), Kaya et al. (2020), and Zhao et al. (2023) based on their mentioned setups. Investing more in the PEMWE system could give more detailed data using an energy monitor from Horizon Educational Group (2023b), including computer software. This investment would have eased up the work of computing the data. Cooperation with Horizon Educational Group could also have been a possibility, requiring knowledge and a more advanced setup. Nevertheless, a contact regarding additional information was not established with Horizon Educational Group, but no response was received.

10 CONCLUSION

Electromagnetic solar radiation can significantly enhance the performance and efficiency of PEMWE due to its energy-carrying photons. These photons possess energy based on their frequency and wavelength. When the photons' energy is channelled into the water-splitting process inside a PEMWE cell, it can excite the electrons within both water molecules and electrode materials. This excitation of the electrons results in a photovoltaic effect, which generates voltage. When the energy of photons is sufficient, they can stimulate the electrons in the water molecules to jump to higher energy levels. Electromagnetic solar radiation can facilitate the stretching and stressing of water molecules, increasing their susceptibility to decompose into H^+ and oxygen. Consequently, the PEM water electrolyser requires less energy to break down the water molecules, as the photons assist in overcoming the activation energy necessary for the water-splitting reaction. This process of water-splitting is a consequence of a photoelectrochemical reaction. The energy from electromagnetic solar radiation also raises the temperature within the PEMWE cell. This temperature rise further supports the water-splitting process. However, the specific impacts of temperature and the photoelectrochemical effect vary based on the electrolyte and materials used in the PEMWE electrolyser. Experimental data from this work shows that electromagnetic solar radiation enhanced the PEM water electrolyser process, leading to a 20% reduction in operational time, a 1.26% voltage increase, a 30.93% increase in current, and consequently, a 31.46% increase in current density compared to the standard condition. Therefore, photoactive cells can drive the water-splitting reaction more efficiently. The success of this process largely depends on the electrolyte and the cell material's capacity to absorb electromagnetic solar radiation, its energy alignment with the water-splitting reaction, and the reaction's rate. A crucial aspect is the activation energy, which the photon-electron interactions can reduce this energy barrier, especially if the photon's energy aligns with or surpasses the bandgap energy. The relationship between photon absorption and activation energy is essential for improving photoactive PEMWE cells.

A magnetic field can significantly enhance the performance and efficiency of PEMWE through the MHD effect, which is the interaction between magnetic fields and conductive fluids. When a conductive fluid flows through a magnetic field, an electromotive force is induced due to the relative motion between the fluid and the magnetic field. The induced electromotive force creates an electric current, generating its own magnetic field. This interaction between the induced electric current and the external magnetic field produces an LF that acts on the fluid, causing motion. FRHR provides a framework for understanding the interaction between MHD and the fundamental principles of electromagnetism

offering an intuitive approach to determining interaction directions between electromotive force, magnetic field, and motion. FRHR can be used to exploit the LF. Consequently, LF can facilitate the removal of oxygen bubbles from the anode in the PEMWE cell and influence the movement of H^+ through the membrane. By ensuring efficient oxygen bubble removal from the anode, the water-splitting process becomes more effective since the transfer of H^+ is enhanced. Experimental data from this work shows when magnetic fields are applied, it challenges the PEM water electrolyser process, leading to a 1.91 % increase in operational time, a 1.22 % voltage decrease, a 3.09 % decrease in current, and consequently, a 6.25 % decrease in current density compared to the standard condition. However, regarding system efficiency, the applied magnetic fields outperformed the standard condition with a 71.98% system efficiency compared to 70.22%. Additionally, the stack potential for applying the magnetic field was 81.34 % compared to 80.35 % for the standard condition. The PEMWE system used for these experimental data had no running flow, impacting the MHD and LF potential. Utilising the full potential of MHD and LF can facilitate the efficient removal of oxygen bubbles, and by the underlying paramagnetic force, from the electrode, reduce concentration polarisation, and, therefore, enhance the productivity of the PEM water electrolyser. Based on the experiments, it was not possible to determine if LF and/or oxygen's paramagnetic attribute drove the bubble removal from the electrode.

Electromagnetic solar radiation has been found to increase the performance of hydrogen production by adding more energy to the system, while magnetic fields are efficient in the transfer and distribution of particles. When these external forces are combined and applied to PEMWE, it results in improved performance and efficiency compared to the standard condition. The combination of electromagnetic solar radiation and magnetic fields led to a 9.70% reduction in operational time, a 1.54% increase in voltage, a 14.18% increase in current, and a 13.81% increase in current density. The effect was not as high as the results obtained with the electromagnetic solar radiation adaption alone. However, the combined adaptation provided better results than the magnetic field adaptation alone. It is important to note that the PEMWE cell used in this study was not designed for these adaptations, which may have impacted the outcome. Further research in PEMWE design is needed to align with the theory and principles of electromagnetic solar radiation and magnetic fields.

REFERENCES

Aoualia, F. Z., Becherif, M., Tabanjat, A., Emzianec, M., Mohammedi, K., Krehid, S., Khellaf, A. 2014. Modelling and experimental analysis of a PEM electrolyser powered by a solar photovoltaic panel. Science Direct. Available at: https://doi.org/10.1016/j.egypro.2014.12.435. Accessed 23.5.2023.

Bidin, N., Azni, S., R., Bakar, M., A., A., Johari., A., R., Munap, D., H., F., A., Salebi, M. F., Razak, S., N., A., Sahidan, N., S., Sulaiman, S., N., A. 2016. The effect of sunlight in hydrogen production from water electrolysis, International Journal of Hydrogen Energy, Volume 42, Issue 1, 2017. Science Direct. Available at: https://doi.org/10.1016/j.ijhydene.2016.11.203. Accessed 24.5.2023.

Bystron, T., Vesely, M., Paidar, M., Papakonstantinou, G., Sundmacher, K., Bensmann, B., Hanke-Rauschenbach R., Bouzek, K. 2018. Enhancing PEM water electrolysis efficiency by reducing the extent of Ti gas diffusion layer passivation. J Appl Electrochem 48, 713–723. Springer Link. Available at: https://doi.org/10.1007/s10800-018-1174-6. Accessed 24.5.2023.

Buitendach H. P. C., Gouws R., Martinson C. A., Minnaar C., Bessarabov D. 2016. Effect of a ripple current on the efficiency of a PEM electrolyser. Science Direct. Available at: https://doi.org/10.1016/j.rineng.2021.100216. Accessed 5.9.2023

Carlton J.S. 2019. Marine Propellers and Propulsion (Fourth Edition), Pages 11-28. Chapter 2 - Propulsion Systems. Science Direct. Available at: https://doi.org/10.1016/B978-0-08-100366-4.00002-X. Accessed 17.8.2023.

Finnish Meteorological Institute. 2023. Diffuse radiation. Available at: https://fmiodata-convert-api-prod.out.ocp.fmi.fi/preview/9076ff06-0c28-4d31-95a2-ff04ac36aed3/?locale=en. Accessed 23.10.2023.

Flowers P., Theopold K., Langley R., Robinson W. R. 2019. Chemistry 2e. OpenStax. Available at https://openstax.org/details/books/chemistry-2e?Book%20details. Accessed 24.7.2023.

Forbes. 2023. Hydrogen Hubs Will Fuel Economic Growth, Especially In Coal Country. Available at: https://www.forbes.com/sites/kensilverstein/2023/10/16/hydrogen-hubs-will-fuel-economic-growth-especially-in-coal-country/?sh=62b97160672c. Accessed 17.10.2023.

Gavlik J. 2014. Horizon Renewable Energy Education Experiment Manual. Available at https://www.scribd.com/document/661319788/Horizon-Renewable-Energy-Education-Experiment-Manual-English-V2-0-. Accessed 30.8.2023.

Gotzig U., Wurdak M., Harmansa N. 2022. Development and coupled thruster / electrolyser tests of a water propulsion system. Acta Astronautica. Volume 202, January 2023, Pages 751-759. Science Direct. Available at: https://doi.org/10.1016/j.actaastro.2022.09.059. Accessed 23.8.2023.

Harun, Tuli N., Mantri A. 2020. Experience Fleming's rule in Electromagnetism Using Augmented Reality: Analyzing Impact on Students Learning. Science Direct. Available at: https://doi.org/10.1016/j.procs.2020.05.086. Accessed 14.8.2023.

Herdem M. A., Mazzeo D., Matera N., Baglivo C., Khan N., Congedo P.M., Giorgi M. G. D. 2023. A brief overview of solar and wind-based green hydrogen production systems: Trends and standardization. Science Direct. Available at: https://doi.org/10.1016/j.ijhydene.2023.05.172. Accessed 17.10.2023.

Horizon Educational Group. 2023a. Solar Hydrogen Science Kit. Available at https://www.horizoneducational.com/solar-hydrogen-science-kit/p1224. Accessed 29.10.2023.

Horizon Educational Group. 2023b. Horizon Energy Monitor. Available at https://www.horizoneducational.com/horizon-energy-monitor/p1220. Accessed 29.10.2023.

Hughes Scott. 2004. Lecture10: Magnetic force; Magnetic fields; Ampere's law. Massachusetts Institute of Technology Department of Physics. Available at https://web.mit.edu/sahughes/www/8.022/lec10.pdf. Accessed 19.10.2023.

Idriss H. 2020. Hydrogen production from water: past and present. Current Opinion in Chemical Engineering. Volume 29, September 2020, Pages 74-82. Science Direct. Available at: https://doi.org/10.1016/j.coche.2020.05.009. Accessed 2.8.2023.

IEA. 2023. Towards hydrogen definitions based on their emissions intensity. International Energy Agency. Available at: https://prod.iea.org/reports/global-hydrogen-review-2023. Accessed 17.10.2023.

Jonasz M., Fournier G. R. 2007. Light Scattering by Particles in Water, Theoretical and Experimental Foundations, Chapter 1 - Basic principles of the interaction of light with matter, pages 1-32. Science Direct. Available at: https://doi.org/10.1016/B978-012388751-1/50001-6. Accessed 24.7.2023.

Kambezidis H. D. 2012. 3.02 - The Solar Resource. Science Direct. Available at: https://doi.org/10.1016/B978-0-08-087872-0.00302-4. Accessed 29.10.2023.

Kaya M. F., Demir N., Rees N. V., El-Kharrouf. 2020. Improving PEM water electrolyser's performance by magnetic field application. Applied Energy. Science Direct. Available at: https://doi.org/10.1016/j.apenergy.2020.114721. Accessed 22.8.2023.

Kong L. B., Liu L., Yang Z., Li S., Zhang T., Wang C. 2018. Magnetic, Ferroelectric, and Multiferroic Metal Oxides. Pages 287-311. 15 - Theory of ferrimagnetism and ferrimagnetic metal oxides. Elsevier. Available at: https://doi.org/10.1016/B978-0-12-811180-2.00015-3. Accessed 11.8.2023.

Kumar S. S., Hankwon L. 2023. Recent advances in hydrogen production through proton exchange membrane water electrolysis – a review. Royal Society of Chemistry. Available at: https://doi.org/10.1039/D3SE00336A. Accessed 17.10.2023.

Kumar S. S., Hankwon L. 2022. An overview of water electrolysis technologies for green hydrogen production. Science Direct. Available at: https://doi.org/10.1016/j.egyr.2022.10.127. Accessed 26.5.2022.

Kumar S. S., Himabindu V. 2019. Hydrogen production by PEM water electrolysis – A review. Science Direct. Available at: https://doi.org/10.1016/j.mset.2019.03.002. Accessed 26.5.2022.

MacCallum R.W., Lewis L.H., Skomski R., Kramer M.J., Anderson I.E. 2014. Practical Aspects of Modern and Future Permanent Magnets. Vol. 44:451-47. Available at: https://doi.org/10.1146/annurev-matsci-070813-113457. Accessed 11.8.2023.

Maier M., Smith K., Dodwell J., Hinds G., Shearing P. R., Brett D.J.L. 2022. Mass transport in PEM water electrolysers: A review. Science Direct. Available at: https://doi.org/10.1016/j.ijhydene.2021.10.013. Accessed 17.10.2023.

Malato-Rodríguez, S. 2004. Solar Detoxification and Disinfection. Encyclopedia of Energy 2004, Pages 587-596. Science Direct. Available at: https://doi.org/10.1016/B0-12-176480-X/00323-5. Accessed 24.7.2023.

Møller K.T., Jensen T.R., Akiba E., Li H. 2016. Hydrogen - A sustainable energy carrier. Science Direct. Available at: https://doi.org/10.1016/j.pnsc.2016.12.014. Accessed 5.9.2023.

Fardell P., Guillaume E. 2010. 11 - Sampling and measurement of toxic fire effluent. Science Direct. Available at: https://www.sciencedirect.com/science/article/abs/pii/B9781845695026500117. Accessed 29.10.2023.

Sheikholeslami M., Ganji D.D. 2016. External Magnetic Field Effects on Hydrothermal Treatment of Nanofluid. Numerical and Analytical Studies. Science Direct. Available at: https://doi.org/10.1016/C2015-0-02006-8. Accessed 13.8.2023.

Speight, J. G. 2018. Reaction Mechanisms in Environmental Engineering, Analysis and Prediction, Chapter 7 -Redox Transformations, pages 231-267. Science Direct. Available at: https://doi.org/10.1016/B978-0-12-804422-3.00007-9. Accessed 18.7.2023.

Speight, J. G. 2017. Environmental Organic Chemistry for Engineers, Chapter 7 - Chemical Transformations in the Environment, pages 305-353. Science Direct. Available at: https://doi.org/10.1016/B978-0-12-804492-6.00007-1. Accessed 22.7.2023.

Tashie-Lewis, B. C., Nnabuife, S. G. 2021. Hydrogen Production, Distribution, Storage and Power Conversion in a Hydrogen Economy - A Technology Review, Chemical Engineering Journal Advances, Volume 8. Science Direct. Available at: https://doi.org/10.1016/j.ceja.2021.100172. Accessed 24.5.2023.

Urone, P. P., Hinrichs R., Dirks K., Sharma M., 2012. College Physics. OpenStax. Available at https://openstax.org/details/books/college-physics. Accessed 17.7.2023.

Whites K.W. 2005. The Electrical Engineering Handbook, Pages 479-497. 1 – Magnetostatics. Science Direct. Available at: https://doi.org/10.1016/B978-012170960-0/50037-2. Accessed 19.8.2023.

WEF. 2023. Everything you need to know about hydrogen in the clean energy transition. World Economic Forum. Available at: https://www.weforum.org/agenda/2023/01/hydrogen-clean-energy-transition-2023#:~:text=Demand%20for%20industrial%20use%20has,progress%20in%20this%20field. Accessed 17.10.2023.

Xing Y., Li H., Avgouropoulos G. 2021. Research Progress of Proton Exchange Membrane Failure and Mitigation Strategies. MDPI. Available at: https://doi.org/10.3390/ma14102591. Accessed 26.5.2023.

Zhang T., Urantani J., Hunag Y., Xu L., Griffiths S. & Ding Y. 2023. Hydrogen liquefaction and storage: Recent progress and perspectives. Renewable and Sustainable Energy Reviews Volume 176. Science Direct. Available at: https://doi.org/10.1016/j.rser.2023.113204. Accessed 27.11.2023.

Zhao P., Wang J., He W., Xia H., Cao X., Li Y., Sun L. 2023. Magnetic field Pre-polarization enhances the efficiency of alkaline water electrolysis for hydrogen production, Energy Conversion and Management, Volume 283. Science Direct. Available at: https://doi.org/10.1016/j.enconman.2023.116906. Accessed 24.5.2023.

APPENDIX 1/1
Raw data from test configurations

Test 1: No alterations @10 ml H2				
Date: 20.10.23	Clock: 15-16:00	Cell surface temperature start/end (˚C): 15.5-16.7		
Time (sec.)	Voltage (V)	Current, I (A)	Resistance (Ohms) R = V/I	Power (Watts) P = V*I
0	1.802	1.098	1.641	1.979
15	1.823	0.888	2.053	1.619
30	1.841	0.845	2.179	1.556
45	1.855	0.811	2.287	1.504
60	1.861	0.779	2.389	1.450
75	1.897	0.749	2.533	1.421
90	1.924	0.770	2.499	1.481
105	2.002	0.630	3.178	1.261
120	2.151	0.490	4.390	1.054
124	2.221	0.439	5.059	0.975
Average	1.938	0.750	2.821	1.430

Test 2: No alterations @10 ml H2				
Date: 20.10.23	Clock: 15-16:00	Cell surface temperature start/end (˚C): 15.5-16.7		
Time (sec.)	Voltage (V)	Current, I (A)	Resistance (Ohms) R = V/I	Power (Watts) P = V*I
0	1.789	0.958	1.867	1.714
15	1.803	0.803	2.245	1.448
30	1.820	0.775	2.348	1.411
45	1.829	0.746	2.452	1.364
60	1.835	0.727	2.524	1.334
75	1.855	0.700	2.650	1.299
90	1.867	0.675	2.766	1.260
105	1.883	0.645	2.919	1.215
120	1.902	0.625	3.043	1.189
135	1.930	0.691	2.793	1.334
Average	1.851	0.735	2.561	1.357

Test 3: No alterations @10 ml H2				
Date: 20.10.23	Clock: 15-16:00	Cell surface temperature start/end (˚C): 15.5-16.7		
Time (sec.)	Voltage (V)	Current, I (A)	Resistance (Ohms) R = V/I	Power (Watts) P = V*I
0	1.779	0.949	1.875	1.688
15	1.791	0.787	2.276	1.410
30	1.803	0.762	2.366	1.374
45	1.799	0.731	2.461	1.315
60	1.803	0.712	2.532	1.284
75	1.813	0.692	2.620	1.255
90	1.833	0.614	2.985	1.125
105	1.844	0.656	2.811	1.210
120	1.860	0.632	2.943	1.176
124	1.859	0.630	2.951	1.171
Average	1.818	0.717	2.582	1.301

Test 4: No alterations @10 ml H2				
Date: 20.10.23	Clock: 15-16:00	Cell surface temperature start/end (˚C): 15.5-16.7		
Time (sec.)	Voltage (V)	Current, I (A)	Resistance (Ohms) R = V/I	Power (Watts) P = V*I
0	1.780	0.922	1.931	1.641
15	1.786	0.803	2.224	1.434
30	1.789	0.764	2.342	1.367
45	1.798	0.738	2.436	1.327
60	1.802	0.779	2.313	1.404
75	1.807	0.700	2.581	1.265
90	1.811	0.682	2.655	1.235
105	1.822	0.668	2.728	1.217
118	1.840	0.642	2.866	1.181
Average	1.804	0.744	2.453	1.341

Test 5: No alterations @10 ml H2				
Date: 20.10.23	Clock: 15-16:00	perature start/end (˚C): 15.5-16.7		
Time (sec.)	Voltage (V)	Current, I (A)	Resistance (Ohms) R = V/I	Power (Watts) P = V*I
0	1.770	0.885	2.000	1.566
15	1.777	0.772	2.302	1.372
30	1.779	0.740	2.404	1.316
45	1.777	0.717	2.478	1.274
60	1.783	0.696	2.562	1.241
75	1.791	0.679	2.638	1.216
90	1.802	0.661	2.726	1.191
105	1.821	0.638	2.854	1.162
120	1.842	0.625	2.947	1.151
128	1.844	0.627	2.941	1.156
Average	1.799	0.704	2.585	1.265

Test 1: Dark field @10 ml H2				
Date: 20.10.23	Clock: 22-23:00	Cell surface temperature start/end (˚C): 15.1-16.3		
Time (sec.)	Voltage (V)	Current, I (A)	Resistance (Ohms) R = V/I	Power (Watts) P = V*I
0	1.716	0.993	1.728	1.704
15	1.802	0.833	2.163	1.501
30	1.802	0.795	2.267	1.433
45	1.804	0.769	2.346	1.387
60	1.807	0.746	2.422	1.348
75	1.812	0.729	2.486	1.321
90	1.818	0.708	2.568	1.287
105	1.827	0.690	2.648	1.261
120	1.839	0.671	2.741	1.234
131	1.847	0.656	2.816	1.212
Average	1.807	0.759	2.418	1.369

Test 2: Dark field @10 ml H2				
Date: 20.10.23	Clock: 22-23:00	Cell surface temperature start/end (˚C): 15.1-16.3		
Time (sec.)	Voltage (V)	Current, I (A)	Resistance (Ohms) R = V/I	Power (Watts) P = V*I
0	1.788	0.911	1.963	1.629
15	1.788	0.793	2.255	1.418
30	1.787	0.751	2.379	1.342
45	1.790	0.725	2.469	1.298
60	1.795	0.704	2.550	1.264
75	1.802	0.685	2.631	1.234
90	1.811	0.667	2.715	1.208
105	1.823	0.648	2.813	1.181
120	1.838	0.638	2.881	1.173
131	1.853	0.624	2.970	1.156
Average	1.808	0.715	2.563	1.290

Test 3: Dark field @10 ml H2				
Date: 20.10.23	Clock: 22-23:00	Cell surface temperature start/end (˚C): 15.1-16.3		
Time (sec.)	Voltage (V)	Current, I (A)	Resistance (Ohms) R = V/I	Power (Watts) P = V*I
0	1.782	0.879	2.027	1.566
15	1.780	0.768	2.318	1.367
30	1.781	0.730	2.440	1.300
45	1.784	0.706	2.527	1.260
60	1.789	0.687	2.604	1.229
75	1.796	0.669	2.685	1.202
90	1.806	0.648	2.787	1.170
105	1.817	0.632	2.875	1.148
120	1.832	0.624	2.936	1.143
135	1.853	0.600	3.088	1.112
Average	1.802	0.694	2.629	1.250

Test 4: Dark field @10 ml H2				
Date: 20.10.23	Clock: 22-23:00	Cell surface temperature start/end (˚C): 15.1-16.3		
Time (sec.)	Voltage (V)	Current, I (A)	Resistance (Ohms) R = V/I	Power (Watts) P = V*I
0	1.764	0.888	1.986	1.566
15	1.778	0.745	2.387	1.325
30	1.781	0.708	2.516	1.261
45	1.783	0.687	2.595	1.225
60	1.789	0.666	2.686	1.191
75	1.799	0.643	2.798	1.157
90	1.808	0.630	2.870	1.139
105	1.824	0.622	2.932	1.135
120	1.840	0.598	3.077	1.100
135	1.863	0.574	3.246	1.069
Average	1.803	0.676	2.709	1.217

Test 5: Dark field @10 ml H2				
Date: 20.10.23	Clock: 22-23:00	Cell surface temperature start/end (˚C): 15.1-16.3		
Time (sec.)	Voltage (V)	Current, I (A)	Resistance (Ohms) R = V/I	Power (Watts) P = V*I
0	1.767	0.899	1.966	1.589
15	1.773	0.739	2.399	1.310
30	1.776	0.688	2.581	1.222
45	1.780	0.668	2.665	1.189
60	1.786	0.642	2.782	1.147
75	1.796	0.630	2.851	1.131
90	1.807	0.622	2.905	1.124
105	1.821	0.601	3.030	1.094
120	1.838	0.580	3.169	1.066
135	1.862	0.558	3.337	1.039
141	1.872	0.480	3.900	0.899
Average	1.807	0.646	2.871	1.165

APPENDIX 1/2

Raw data from test configurations

Test 1: Solar @10 ml H2				
Date: 21.10.23	Clock: 13-14:00	Cell surface temperature start/end (˚C): 18.5-19.9		
me (sec.)	Voltage (V)	Current, I (A)	Resistance (Ohms) R = V/I	Power (Watts) P = V*I
0	1.804	1.262	1.429	2.277
15	1.801	1.030	1.749	1.855
30	1.861	1.053	1.767	1.960
45	1.865	1.005	1.856	1.874
60	1.869	0.943	1.982	1.762
75	1.883	0.930	2.025	1.751
90	1.900	0.901	2.109	1.712
99	1.901	0.882	2.156	1.677
Average	1.861	1.001	1.884	1.649

Test 2: Solar @10 ml H2				
Date: 21.10.23	Clock: 13-14:00	Cell surface temperature start/end (˚C): 18.5-19.9		
me (sec.)	Voltage (V)	Current, I (A)	Resistance (Ohms) R = V/I	Power (Watts) P = V*I
0	1.809	1.172	1.544	2.120
15	1.839	1.050	1.751	1.931
30	1.841	0.993	1.854	1.828
45	1.857	0.956	1.942	1.775
60	1.873	0.924	2.027	1.731
75	1.894	0.888	2.133	1.682
90	1.922	0.846	2.272	1.626
96	1.936	0.825	2.347	1.597
Average	1.871	0.957	1.984	1.786

Test 3: Solar @10 ml H2				
Date: 21.10.23	Clock: 13-14:00	Cell surface temperature start/end (˚C): 18.5-19.9		
me (sec.)	Voltage (V)	Current, I (A)	Resistance (Ohms) R = V/I	Power (Watts) P = V*I
0	1.848	1.185	1.559	2.190
15	1.848	1.050	1.760	1.940
30	1.848	0.992	1.863	1.833
45	1.854	0.954	1.943	1.769
60	1.864	0.924	2.017	1.722
75	1.877	0.890	2.109	1.671
90	1.898	0.858	2.212	1.628
101	1.919	0.824	2.329	1.581
Average	1.870	0.960	1.974	1.792

Test 4: Solar @10 ml H2				
Date: 21.10.23	Clock: 13-14:00	Cell surface temperature start/end (˚C): 18.5-19.9		
me (sec.)	Voltage (V)	Current, I (A)	Resistance (Ohms) R = V/I	Power (Watts) P = V*I
0	1.771	1.187	1.492	2.102
15	1.848	1.032	1.791	1.907
30	1.849	0.979	1.889	1.810
45	1.853	0.945	1.961	1.751
60	1.863	0.914	2.038	1.703
75	1.877	0.883	2.126	1.657
90	1.899	0.850	2.234	1.614
102	1.925	0.816	2.359	1.571
Average	1.861	0.951	1.986	1.764

Test 5: Solar @10 ml H2				
Date: 21.10.23	Clock: 13-14:00	Cell surface temperature start/end (˚C): 18.5-19.9		
me (sec.)	Voltage (V)	Current, I (A)	Resistance (Ohms) R = V/I	Power (Watts) P = V*I
0	1.854	1.156	1.604	2.143
15	1.841	0.992	1.856	1.826
30	1.842	0.925	1.991	1.704
45	1.847	0.911	2.027	1.683
60	1.858	0.882	2.107	1.639
75	1.859	0.833	2.232	1.549
90	1.892	0.804	2.353	1.521
102	1.916	0.777	2.466	1.489
Average	1.864	0.910	2.079	1.694

Test 1: Solar & Magnets @10 ml H2				
Date: 22.10.23	Clock: 14-15:00	Cell surface temperature start/end (˚C): 18.0-19.7		
e (sec.)	Voltage (V)	Current, I (A)	Resistance (Ohms) R = V/I	Power (Watts) P = V*I
0	1.860	1.112	1.673	2.069
15	1.830	0.998	1.834	1.826
30	1.834	0.954	1.922	1.750
45	1.839	0.917	2.005	1.686
60	1.849	0.885	2.089	1.636
75	1.868	0.856	2.182	1.599
90	1.887	0.819	2.304	1.545
104	1.918	0.780	2.459	1.496
Average	1.861	0.915	2.059	1.701

Test 2: Solar & Magnets @10 ml H2				
Date: 22.10.23	Clock: 14-15:00	Cell surface temperature start/end (˚C): 18.0-19.7		
e (sec.)	Voltage (V)	Current, I (A)	Resistance (Ohms) R = V/I	Power (Watts) P = V*I
0	1.842	1.073	1.717	1.976
15	1.840	0.950	1.937	1.748
30	1.840	0.898	2.049	1.652
45	1.846	0.864	2.137	1.595
60	1.858	0.833	2.230	1.548
75	1.875	0.803	2.335	1.506
90	1.904	0.764	2.492	1.455
105	1.943	0.719	2.702	1.397
110	1.960	0.700	2.800	1.372
Average	1.879	0.845	2.267	1.583

Test 3: Solar & Magnets @10 ml H2				
Date: 22.10.23	Clock: 14-15:00	Cell surface temperature start/end (˚C): 18.0-19.7		
e (sec.)	Voltage (V)	Current, I (A)	Resistance (Ohms) R = V/I	Power (Watts) P = V*I
0	1.840	1.053	1.747	1.938
15	1.836	0.913	2.011	1.676
30	1.842	0.867	2.125	1.597
45	1.854	0.829	2.236	1.537
60	1.873	0.790	2.371	1.480
75	1.904	0.750	2.539	1.428
90	1.948	0.696	2.799	1.356
105	1.999	0.627	3.188	1.253
120	1.999	0.543	3.681	1.085
Average	1.899	0.785	2.522	1.483

Test 4: Solar & Magnets @10 ml H2				
Date: 22.10.23	Clock: 14-15:00	Cell surface temperature start/end (˚C): 18.0-19.7		
e (sec.)	Voltage (V)	Current, I (A)	Resistance (Ohms) R = V/I	Power (Watts) P = V*I
0	1.769	1.017	1.739	1.799
15	1.814	0.901	2.013	1.634
30	1.816	0.854	2.126	1.551
45	1.822	0.822	2.217	1.498
60	1.835	0.793	2.314	1.455
75	1.853	0.766	2.419	1.419
90	1.879	0.739	2.543	1.389
105	1.917	0.688	2.786	1.319
114	1.946	0.656	2.966	1.277
Average	1.850	0.804	2.347	1.482

Test 5: Solar & Magnets @10 ml H2				
Date: 22.10.23	Clock: 14-15:00	Cell surface temperature start/end (˚C): 18.0-19.7		
e (sec.)	Voltage (V)	Current, I (A)	Resistance (Ohms) R = V/I	Power (Watts) P = V*I
0	1.885	1.053	1.790	1.985
15	1.817	0.908	2.001	1.650
30	1.817	0.861	2.110	1.564
45	1.822	0.829	2.198	1.510
60	1.893	0.801	2.363	1.516
75	1.849	0.774	2.389	1.431
90	1.864	0.745	2.502	1.389
105	1.892	0.709	2.669	1.341
120	1.929	0.675	2.858	1.302
Average	1.863	0.817	2.320	1.521

APPENDIX 1/3

Raw data from test configurations

Test 1: Magnets @10 ml H2				
Date: 22.10.23	Clock: 15-16:00	Cell surface temperature start/end (˚C): 15.5-16.3		
Time (sec.)	Voltage (V)	Current, I (A)	Resistance (Ohms) R = V/I	Power (Watts) P = V*I
0	1.750	0.930	1.882	1.628
15	1.795	0.846	2.122	1.519
30	1.800	0.825	2.182	1.485
45	1.802	0.795	2.267	1.433
60	1.807	0.774	2.335	1.399
75	1.813	0.753	2.408	1.365
90	1.821	0.730	2.495	1.329
105	1.832	0.708	2.588	1.297
119	1.848	0.685	2.698	1.266
Average	1.808	0.783	2.330	1.413

Test 2: Magnets @10 ml H2				
Date: 22.10.23	Clock: 15-16:00	Cell surface temperature start/end (˚C): 15.5-16.3		
Time (sec.)	Voltage (V)	Current, I (A)	Resistance (Ohms) R = V/I	Power (Watts) P = V*I
0	1.756	1.032	1.702	1.812
15	1.794	0.829	2.164	1.487
30	1.795	0.785	2.287	1.409
45	1.799	0.758	2.373	1.364
60	1.806	0.735	2.457	1.327
75	1.815	0.714	2.542	1.296
90	1.832	0.690	2.655	1.264
105	1.854	0.666	2.784	1.235
120	1.882	0.630	2.987	1.186
122	1.887	0.629	3.000	1.187
Average	1.822	0.747	2.495	1.357

Test 3: Magnets @10 ml H2				
Date: 22.10.23	Clock: 15-16:00	Cell surface temperature start/end (˚C): 15.5-16.3		
Time (sec.)	Voltage (V)	Current, I (A)	Resistance (Ohms) R = V/I	Power (Watts) P = V*I
0	1.788	0.956	1.870	1.709
15	1.788	0.801	2.232	1.432
30	1.788	0.759	2.356	1.357
45	1.792	0.733	2.445	1.314
60	1.799	0.712	2.527	1.281
75	1.810	0.693	2.612	1.254
90	1.826	0.671	2.721	1.225
105	1.846	0.643	2.871	1.187
120	1.875	0.622	3.014	1.166
129	1.896	0.603	3.144	1.143
Average	1.821	0.719	2.579	1.307

Test 4: Magnets @10 ml H2				
Date: 22.10.23	Clock: 15-16:00	Cell surface temperature start/end (˚C): 15.5-16.3		
Time (sec.)	Voltage (V)	Current, I (A)	Resistance (Ohms) R = V/I	Power (Watts) P = V*I
0	1.766	0.916	1.928	1.618
15	1.779	0.769	2.313	1.368
30	1.780	0.732	2.432	1.303
45	1.782	0.706	2.524	1.258
60	1.790	0.688	2.602	1.232
75	1.800	0.671	2.683	1.208
90	1.812	0.648	2.796	1.174
105	1.832	0.629	2.913	1.152
120	1.856	0.614	3.023	1.140
126	1.869	0.598	3.125	1.118
Average	1.807	0.697	2.634	1.257

Test 5: Magnets @10 ml H2				
Date: 22.10.23	Clock: 15-16:00	Cell surface temperature start/end (˚C): 15.5-16.3		
Time (sec.)	Voltage (V)	Current, I (A)	Resistance (Ohms) R = V/I	Power (Watts) P = V*I
0	1.773	0.750	2.364	1.330
15	1.779	0.687	2.590	1.222
30	1.777	0.654	2.717	1.162
45	1.783	0.630	2.830	1.123
60	1.793	0.621	2.887	1.113
75	1.809	0.601	3.010	1.087
90	1.828	0.579	3.157	1.058
105	1.856	0.551	3.368	1.023
120	1.894	0.511	3.706	0.968
135	1.951	0.477	4.090	0.931
145	1.999	0.433	4.617	0.866
Average	1.840	0.590	3.212	1.080

APPENDIX 2

Current density data and calculations.

No alterations (10 points in time), Voltage (V) vs. Current density (A/cm²), 10 ml H_2 @ 125.8 sec.			
Time (sec.)	Voltage (V)	Current, I (A)	Current density (A/cm²)
0.0	1.784	0.962	0.167
15.0	1.796	0.811	0.141
30.0	1.806	0.777	0.135
45.0	1.812	0.749	0.130
60.0	1.817	0.739	0.128
75.0	1.833	0.704	0.122
90.0	1.847	0.680	0.118
105.0	1.874	0.647	0.113
119.6	1.919	0.603	0.105
127.8	1.964	0.597	0.104
Average	1.845	0.727	0.126

Dark field (11 points in time), Voltage (V) vs. Current density (A/cm²), 10 ml H_2 @ 134.6 sec.			
Time (sec.)	Voltage (V)	Current, I (A)	Current density (A/cm²)
0.0	1.763	0.914	0.159
15.0	1.784	0.776	0.135
30.0	1.785	0.734	0.128
45.0	1.788	0.711	0.124
60.0	1.793	0.689	0.120
75.0	1.801	0.671	0.117
90.0	1.810	0.655	0.114
105.0	1.822	0.639	0.111
120.0	1.837	0.622	0.108
133.4	1.856	0.602	0.105
141.0	1.872	0.480	0.083
Average	1.810	0.681	0.118

Solar (8 points in time), Voltage (V) vs. Current density (A/cm²), 10 ml H_2 @ 100.0 sec.			
Time (sec.)	Voltage (V)	Current, I (A)	Current density (A/cm²)
0.0	1.817	1.192	0.207
15.0	1.835	1.031	0.179
30.0	1.848	0.988	0.172
45.0	1.855	0.954	0.166
60.0	1.865	0.917	0.160
75.0	1.878	0.885	0.154
90.0	1.902	0.852	0.148
100.0	1.919	0.825	0.143
Average	1.865	0.956	0.166

Solar & Magnets (9 points in time), Voltage (V) vs. Current density (A/cm²), 10 ml H_2 @ 113.6 sec.			
Time (sec.)	Voltage (V)	Current, I (A)	Current density (A/cm²)
0.0	1.839	1.062	0.185
15.0	1.827	0.934	0.162
30.0	1.830	0.887	0.154
45.0	1.837	0.852	0.148
60.0	1.862	0.820	0.143
75.0	1.870	0.790	0.137
90.0	1.896	0.753	0.131
104.8	1.934	0.705	0.123
116.0	1.959	0.644	0.112
Average	1.873	0.827	0.144

Magnets (11 points in time), Voltage (V) vs. Current density (A/cm²), 10 ml H_2 @ 128.2 sec.			
Time (sec.)	Voltage (V)	Current, I (A)	Current density (A/cm²)
0.0	1.767	0.917	0.159
15.0	1.787	0.786	0.137
30.0	1.788	0.751	0.131
45.0	1.792	0.724	0.126
60.0	1.799	0.706	0.123
75.0	1.809	0.686	0.119
90.0	1.824	0.664	0.115
105.0	1.844	0.639	0.111
119.8	1.871	0.612	0.107
128.0	1.901	0.577	0.100
145.0	1.999	0.433	0.075
Average	1.835	0.681	0.119